LIBRARY
ROYAL AIRCRAFT ESTABLISHMENT
BEDFORD.

R. & M. No. 3129
(19,629)
A.R.C. Technical Report

MINISTRY OF SUPPLY

AERONAUTICAL RESEARCH COUNCIL
REPORTS AND MEMORANDA

Low-Speed Wind-Tunnel Tests on the De Havilland *Sea Venom* with Blowing over the Flaps

By

S. F. J. Butler and M. B. Guyett

© *Crown copyright 1959*

LONDON: HER MAJESTY'S STATIONERY OFFICE
1959
PRICE £1 0s. 0d. NET

Low-Speed Wind-Tunnel Tests on the De Havilland *Sea Venom* with Blowing over the Flaps

By

S. F. J. Butler and M. B. Guyett

Communicated by the Director-General of Scientific Research (Air), Ministry of Supply

Reports and Memoranda No. 3129*

February, 1957

Summary.—This report contains the results of low-speed tunnel tests of longitudinal stability on a modified *Sea Venom* Mk. 21 fitted with blowing over the flaps. At each flap angle, a range of values of the sectional momentum coefficient was tested. As a typical example, the increase in trimmed C_L at constant incidence resulting from blowing at flaps 60 deg was about $0 \cdot 45$, the increase in $C_{L\max}$ being somewhat smaller. The equivalent reduction in approach speed of 10 to 15 kt predicted from the tunnel results was later achieved in flight. The tunnel results suggested a beneficial reduction in minimum-drag speed due to blowing, particularly at large flap angles. Trim changes were large, amounting to about 8 deg on the all-movable tail at flaps 60 deg.

A comparison is made between estimated and measured effects of blowing. It is shown that, whilst the lift and pitching-moment increments resulting from flap blowing can be estimated fairly closely, the drag increments at large flap angles are much larger than would be expected. The additional drag tends to decrease the minimum-drag speed and increase the minimum drag, and may affect the take-off and landing performance appreciably. The effect will be unfavourable in the first case and favourable in the second.

A flight/tunnel comparison is included of the lift increments resulting from blowing. At flaps 40 deg, agreement is good, but at larger flap angles, the lift increments measured in flight were less than those measured on the model. Possible reasons for this are discussed. There is a favourable Reynolds-number effect on $C_{L\max}$ which is found to be somewhat larger for the blown flap than for the unblown flap.

1. *Introduction.*—This report supersedes the preliminary note[1] already issued and contains a full discussion of the results of low-speed longitudinal-stability tests on a 2/7th scale half-model of the De Havilland *Sea Venom* with blowing over trailing-edge flaps.

A comparison is made between the measured and estimated effects of blowing. A comparison is also made between the model results and the results of subsequent flight tests.

2. *Model Details.*—A 2/7th-scale half-model of the De Havilland *Sea Venom* Mk. 21 was mounted on the lower balance of the Royal Aircraft Establishment No. 2, $11\frac{1}{2}$ ft $\times$ $8\frac{1}{2}$ ft Wind Tunnel. The model (which was manufactured by Messrs. De Havillands), was largely made from mahogany with a phenoglaze finish; the blowing ducts and nozzles were made in mild steel,

* R.A.E. Report Aero. 2587, received 5th November, 1957.

Duralumin and brass. Most of the tests were made with a fairing over the engine intake; this fairing was removed for tests with simulated engine-intake conditions at take-off and landing. For simplicity, an all-moving tail was provided in place of the normal tail unit.

In order to represent the modified *Sea Venom* which is being flown with a flap-blowing installation, the tip tank, leading-edge slat, boundary-layer fence, and drooped wing leading edge were fitted on the model. In the full-scale application, engine air is ducted directly into the flaps and discharged tangentially through a slot in the flap nose, the nozzle position therefore rotating with the flaps. On the model, however, it was more convenient to duct the air through the wing to cavities between the wing and the flap, whence it was discharged over the flaps (*see* Fig. 4); thus it was not possible to simulate the airflow through the wing-flap gap which occurred on the aircraft. The likely effects of this and other differences between the aircraft and the model are discussed in Section 8.

The flaps could be set at 20-deg intervals from 0 to 80 deg. For the 40-deg and 60-deg cases, several nozzle positions at 20-deg intervals round the noses of the flaps were tested by using a range of cover plates (*see* Figs. 2, 3 and 4). Thus the results can be used to estimate the relative performances of a shroud-blowing installation (in which the nozzle is fixed in the wing ahead of the flap), and a flap-blowing installation (in which the nozzle is fixed in the flap nose and rotates with the flap).

The blowing tests were done at two pressure ratios, $1 \cdot 9 : 1$ and $2 \cdot 9 : 1$, corresponding respectively to landing and take-off conditions. The blowing-momentum coefficient, C_μ', could also be varied by changing the nozzle depth, which was regulated by spacers at intervals across the span of the nozzle occupying in all about 13 per cent of the nozzle span (*see* Fig. 2), or by changing the tunnel speed.

The tests were generally made at 180 ft/sec, corresponding to a Reynolds number, based on aerodynamic mean chord, of $2 \cdot 7 \times 10^6$ ($2 \cdot 5 \times 10^6$ when based on standard mean chord). The tests were carried out between March and August, 1955.

3. *Test Procedure*.—3.1. *Leak Tests*.—Some large leaks in the pressure boxes were sealed satisfactorily with cold-setting Araldite. Subsequent leak tests made under operational conditions showed the remaining leaks amounted to 1 per cent of the minimum flow rate to be used, and this was considered to be acceptable.

3.2. *Effect of Air Supply on Balance Zeros*.—The air supply line to the model for flap blowing consisted of three distinct portions. The supply pipe from the compressors ended in a short vertical pipe on the common axis of rotation of the balance and the tunnel turn-table. This pipe was connected, *via* a rotating air-tight joint, to another short vertical pipe suspended rigidly by a stirrup plate attached to the tunnel turn-table. The final, flexible, connection to the model was made by a constricted canvas sleeve. The model and turn-table were rotated together so that the canvas sleeve remained untwisted, and the model incidence could be altered whilst the tunnel was running and air was being discharged over the flaps.

Valves on either side of the sleeve allowed this portion to be pressurised to the correct static pressure whilst zeros were being taken for the blow-on runs. Zeros taken in this way differed from the unpressurised zeros by 2 to 4 lb (lift and drag) and 1 lb ft (pitching moment), corresponding to $0 \cdot 004$ to $0 \cdot 008$ (C_L and C_D) and $0 \cdot 001$ (C_m). Consequently, zeros for blow-on runs had to be taken with the correct static-pressure conditions in the sleeve. These zeros were found to be repeatable and consistent to a high order of accuracy, and the zero scatter was only slightly greater than that which would have occurred with a conventional model on this balance.

For a full discussion of the air supply arrangement, the reader is referred to Ref. 2.

3.3. *Definition and Measurement of Blowing-Momentum Coefficient, and Range of Values Covered.*—The normal definition is used for the sectional momentum coefficient, C_μ', in terms of the mass-flow rate and the jet velocity after isentropic expansion to free-stream pressure. It may be calculated from the pressure ratio and cross-sectional area of the nozzle:

$$C_\mu' = \frac{3\cdot840 \times 10^3}{\frac{1}{2}\rho_0 U_0^2} \frac{S''}{S'} \frac{p_D}{p_0} \left\{1 - \left(\frac{p_0}{p_D}\right)^{2/7}\right\}^{1/2} \qquad \left(\frac{p_D}{p_0} > 1\cdot893\right)$$

and

$$C_\mu' = \frac{1\cdot484 \times 10^4}{\frac{1}{2}\rho_0 U_0^2} \frac{S''}{S'} \left\{\left(\frac{p_D}{p_0}\right)^{2/7} - 1\right\} \qquad \left(\frac{p_D}{p_0} < 1\cdot893\right)$$

or, alternatively, from the pressure ratio and the measured mass flow rate:

$$C_\mu' = \frac{4\cdot572 m T_D^{1/2}}{\frac{1}{2}\rho_0 U_0^2 S'} \left\{1 - \left(\frac{p_0}{p_D}\right)^{2/7}\right\}^{1/2}.$$

The symbols and units are defined in the List of Symbols at the end of the text. The momentum coefficient, C_μ, based on gross wing area, can be obtained from C_μ' by writing $C_\mu = C_\mu'(S'/S)$.

In order to measure the momentum coefficient on the tunnel model, it was therefore necessary either to know the pressure ratio and the throat area of the nozzle (assuming full flow in the nozzle), or else the pressure ratio and the mass-flow rate. Both methods were in fact used. The spanwise distribution of total head at the nozzle was calibrated against a static tapping inside the wing-flap cavity, the latter being used during test runs to determine the pressure ratio. The throat area of the nozzle was calculated from the net span of the nozzle and the average depth; the latter was checked by feeler traverses. The mass-flow rate was measured by standard orifice plates inserted in the supply lines. The alternative methods were generally in good agreement.

Typical spanwise variations in nozzle depth and total head, p_D, are shown in Fig. 7 for the model. It is thought that the small variations found were unlikely to have a large adverse effect on the results. In any case, the flight installation showed much larger spanwise variations in p_D and hence in the resulting momentum distribution (*see* Section 8 and Fig. 8).

The formulae given above show how the sectional momentum coefficient, C_μ', could be varied by altering one of the three test variables, namely, nozzle depth, pressure ratio, or wind speed. The most convenient control was usually the pressure ratio, and the tests were mainly made at 180 ft/sec, with a 0·035-in. nozzle depth. Over the limited range covered in these tests, it was found that the effects of blowing were functions of the momentum coefficient, and were independent of the method used to obtain variations of the momentum coefficient; a similar result has been found in other tests (for example, *see* Ref. 4).

The range of conditions tested is summarised in the following Table:

Nominal wind speed (ft/sec)	Mean nozzle depth (in.)	Pressure ratio	Sectional momentum coefficient, C_μ'
180	0·021	1·9 : 1	0·046
	0·035	1·9 : 1 2·9 : 1	0·077 0·154
140	0·035	1·9 : 1 2·9 : 1	0·132 0·264

The sectional momentum coefficient available during the aircraft approach was expected to be about $C_\mu' = 0\cdot077$, at which value most of the tunnel tests were done; for the baulked landing and at take-off, a value of $0 \cdot 154$ for C_μ' could be attained. Tests were also made at $C_\mu' = 0 \cdot 046$ to ensure that $C_\mu' = 0 \cdot 077$ did not correspond to a marginally attached flow, and also in case the momentum coefficient available on the aircraft was below estimate.

3.4. *Corrections*.—Blockage corrections to $\frac{1}{2}\rho_0 U_0^2$ have been calculated, using a new method[3] which allows for increased wake blockage when separations are present. It was found to be no longer satisfactory to apply a constant blockage correction to all results; a graduated allowance for blockage has been made as illustrated by the following Table:

Flaps (deg)	Percentage correction to $\frac{1}{2}\rho_0 U_0^2$		
	Low incidences	At the stall	Above the stall
0, 40	1	2	up to 10
60, 80	3	4	

The following tunnel-constraint corrections were subsequently applied, all being added:

$$\Delta\alpha = 0 \cdot 99 C_{L\,(\text{No-tail})}$$

$$\Delta C_D = 0 \cdot 0173 C_{L\,(\text{No-tail})}^2$$

(Tail-on runs) $$\Delta C_m = -\,0 \cdot 53 \frac{dC_m}{d\eta_T} C_{L\,(\text{No-tail})} \qquad (\eta_T \text{ in deg}) .$$

4. *Test Results*.—The test results are given in Tables 2 to 4 and described in this Section. Table 2, which is headed by a description of the standard model configuration, contains the main results. Table 3 contains brief results obtained with the tail boom removed and the local wing trailing edge faired. Table 4 contains the results of auxiliary tests to determine the effect of various modifications to the standard model configuration.

Most of the tests were made with both flaps deflected, and with blowing from nozzle position 2 (*see* Fig. 4), corresponding to the nozzle position used on the aircraft. These tests are described in Section 4.1. At flaps 40 and 60 deg, tests were made at other fore-and-aft positions of the nozzle (*see* Section 4.2). At flaps 60 deg, tests were made to compare the performance of the normal parallel blowing slit with blowing through a series of discrete circular nozzles (*see* Section 4.3).

In order to help the analysis of the lift and drag increments produced by two part-span flaps, a comparison is made in Section 4.4 between blowing over the outboard flap only, with the inboard flap undeflected, and blowing over both flaps. This section also contains a discussion of the effect of removing the boom on the performance of the outboard flap. This test was essential to determine the unknown effect of the boom on the blown flap, since it was desired to make a comparison between the measured and the estimated effects of blowing.

The remaining Sections, 4.5 to 4.9, describe the results of various modifications to the standard test condition.

4.1. *The Effect of Blowing over both Flaps at Nozzle Position* 2 (*Flaps* 40, 60 *and* 80 *deg*).—In this Section, the results obtained with the standard model configuration (*see* Table 2) at nozzle position 2 are discussed. Nozzle position 2 (*see* Fig. 4), which corresponds closely to the position chosen for the aircraft, is fixed relative to the flap, and so rotates with the flap as the latter is deflected, being located at 20, 40 and 60 deg round the nose of the flap at flap angles of 40, 60 and 80 deg respectively. The other nozzle positions, 1 and 3, are respectively 20 deg further aft and 20 deg further forward than position 2.

4.1.1. *Lift and stalling behaviour*.—The variation of $C_{L\,(\text{No-tail})}$ and $C_{L\,(\text{Trimmed})}$ with wing incidence, α, is shown in Figs. 9a to 9c for a range of momentum coefficient, C_μ', at each flap angle. The combined effect of flap angle and momentum coefficient on $C_{L\,(\text{No-tail})}$ versus α is given in Fig. 9d. The momentum coefficient, C_μ', is based on the 'blown' area of the wing, S' (*i.e.*, the area of the wing spanned by the flaps), and therefore corresponds to the sectional momentum coefficient used in two-dimensional tests (when $C_\mu \equiv C_\mu'$).

At each flap angle, there was the anticipated increase with C_μ' in the lift coefficient at constant incidence. The rate of increase of flap lift with C_μ' was, as would be expected, greater at the lower values of C_μ' (when separations were being suppressed by the blowing jet), than at higher values of C_μ'. There was a tendency for $dC_L/d\alpha$ to increase slightly on the application of blowing at low flap angles.

The stalling incidence was generally only decreased slightly by blowing. This was consistent with tuft observations which showed that the wing stalling behaviour did not appear to be affected by blowing. The wing leading edge was drooped to avoid any leading-edge separations which otherwise might have resulted from high sectional loading over the portion of the wing spanned by the flaps. Under all conditions, the wing was found to stall by rear separations.

The only case where the application of blowing caused a substantial change in the stalling incidence was at flaps 80 deg, $C_\mu' = 0{\cdot}077$. In this case, tufts showed that the outboard flap stalled prematurely as the incidence was increased, presumably because of the comparatively low value for C_μ' in view of the large flap angle. In order to obtain the curve shown in Fig. 9c for this condition, blowing was applied to the model at zero incidence before running the tunnel up to speed, and the incidence range was then covered at the correct value of $0{\cdot}077$ for C_μ'. It was found, however, that once the outboard flap had been stalled by exceeding $\alpha = 14$ deg, the flow could not be reattached to the flap at this value of C_μ', even if the model incidence was reduced to zero again. Similarly, if the tunnel was run up to speed at $C_\mu' = 0$, and blowing applied subsequently, the outboard flap remained stalled, unless the value of $0{\cdot}077$ for C_μ' was considerably exceeded. On the other hand, at $C_\mu' = 0{\cdot}154$, flaps 80 deg, and at all the values of C_μ' tested at lower flap angles, it was immaterial whether blowing was applied before starting the tunnel or after attaining the test speed, and it was also possible to reattach the flow over the flap by decreasing incidence after stalling the wing, without any signs of hysteresis.

Fig. 13 shows the variation with C_μ' of $\Delta C_{L\,(\text{Flap + Blow})}$ and $\Delta C_{L\,(\text{Blow})}$ for different flap angles at $\alpha = 5$ deg, a representative constant incidence. Fig. 14 shows the corresponding variation with C_μ' of $C_{L\,\max}$, $\Delta C_{L\,\max\,(\text{Flap + Blow})}$, and $\Delta C_{L\,\max\,(\text{Blow})}$. In each figure, both no-tail and trimmed values are shown. The values for $\Delta C_{L\,(\text{Flap + Blow})}$ at $\alpha = 5$ deg (no-tail) are compared with estimate in Section 5.1. Predictions of the effect of blowing on stalling, take-off, and approach speeds are given in Section 6. Finally, differences between the lift increments measured in the tunnel tests and in the flight tests are discussed in Section 8.2.

Table 2 includes some brief tests obtained with blowing at zero flap angle. The model was not designed for this case and some discontinuity had to be made in the upper wing profile in the region of the nozzle, in order to test this condition. Hence, too much emphasis should not be placed on the low thrust-recovery factor obtained from these tests. The results at zero flap angle, however, do show an increase in lift slope, and an increase in lift at zero incidence when blowing is applied.

4.1.2. *Drag*.—The variation of C_D with C_L is shown in Figs. 10a to 10c for a range of C_μ' at each flap angle for the no-tail condition. The combined effect of flap angle and C_μ' is shown in Fig. 10d. The drag coefficients shown include any component of jet thrust recovered*.

At flaps 40 deg, the curves for different values of C_μ' lie close together. Thus, the increase in flap-induced drag was balanced at this flap angle by the jet thrust recovered, plus reductions in flap profile drag resulting from the suppression of flap separations.

* No allowance has been made for 'sink' effects on drag coefficients associated with delivering blowing air to the model instead of using main-stream air. The effects would be small in the present case.

At flaps 60 and 80 deg, however, there were substantial increases in drag coefficient at constant C_L on the application of blowing. Some minor increases would be expected, as a result of additional flap-induced drag and the reduced jet thrust recovered. However, it will be shown later (Section 5.2) that the measured increases were much larger than the increases predicted by the normal methods of estimation.

The effect of blowing on minimum drag and minimum-drag speeds is discussed in Section 7.

4.1.3. *Pitching moments.*—Pitching moments were measured about 28·3 per cent aerodynamic mean chord (28·5 per cent standard mean chord). The pitching-moment axis was 0·043 ft (model scale) above the centre-line wing chord.

The variation of C_m with C_L is shown in Figs. 11a to 11c for a range of C_μ' at each flap angle; the combined effect of flap angle and C_μ' is given in Fig. 11d. Fig. 12 shows the variation of mean downwash at the tail position and tail-setting angle to trim with α for a range of C_μ' at each flap angle (note that the tail angle is fixed on the aircraft and trimming obtained by deflection of an elevator).

The application of blowing resulted in large nose-down pitching-moment changes in the no-tail condition. The magnitude of $(\Delta C_m/\Delta C_L)_{(\mathrm{Flap}\,+\,\mathrm{Blow})}$ is compared in Section 5.3 with estimates based on Ref. 4. With the tail on, the increased downwash at the tail tends to alleviate the trimming required. Nevertheless, the application of blowing at flaps 60 deg requires an 8-deg negative trim change of the all-movable tail, relative to the unblown flap.

Below the stall, the application of blowing tends to reduce the stability by a small amount. For the sake of clarity, only a few of the pitching-moment curves have been plotted beyond the stall; further data showing the stalling behaviour can be found in the Tables. With blow on, at the stall there is initially a mild pitch-up, followed by a nose-down stall in contrast to the nose-down stall without pitch-up for the unblown flap. In the case $C_\mu' = 0 \cdot 077$, flaps 80 deg (Fig. 11c), the pitch-up is more severe as a result of the premature stall of the outboard flap (*see* Section 4.1.1), which results in a reduction in $\Delta C_{L\,(\mathrm{Blow})}$ accompanied by a corresponding reduction in the magnitude of $\Delta C_{m\,(\mathrm{Blow})}$.

4.2. *The Effect of Nozzle Position* (*Flaps* 40 *and* 60 *deg*).—Throughout this report, apart from this Section, the results are quoted for nozzle position 2, which corresponds closely to the position chosen for the aircraft. As can be seen from Fig. 4, position 2 is fixed relative to the flap and rotates with the flap. It is located 20, 40 and 60 deg round the flap nose from the vertical at flap angles of 40, 60 and 80 deg respectively. Position 1 is 20 deg further aft and position 3 is 20 deg further forward than position 2. At flaps 60 deg, all three positions were tested; at flaps 40 deg, positions 1 and 2 were tested. The results are presented in Figs. 15a to 15d.

At flaps 40 deg, the lift increments due to blowing (*see* Fig. 15d) were virtually the same whichever position was used, and there were no significant effects on the other coefficients.

At flaps 60 deg (*see* Figs. 15a to 15c), position 3 was found to be inferior to the other two positions, particularly at the lower value of C_μ' (0·046). The lift increments at $\alpha = 5$ deg are shown in Fig. 15d. For $C_\mu' = 0 \cdot 046$, the value of $\Delta C_{L\,(\mathrm{Blow})}$ was 0·29 at position 3 compared with 0·41 at positions 1 and 2, so that there was a variation of 0·12 in the lift increment for the three positions tested. By $C_\mu' = 0 \cdot 077$, the variation in the lift increment at $\alpha = 5$ deg had fallen to 0·03.

The drag curves (Fig. 15b) show, at $C_\mu' = 0 \cdot 046$, similar variations with the position of the nozzle. The C_D vs. C_L curve for position 3, where the lift increment produced by blowing was inferior, lies below the curves for positions 1 and 2. Since the drag increments produced by blowing (*see* Section 5.2 and Ref. 10) are thought to be associated with the attainment of attached flow, these drag effects are of the type which would be expected. At $C_\mu' = 0 \cdot 077$, where almost the same lift increments were produced at each of the three positions tested, the drag curves are much closer together. The nose-down pitching-moment increments (*see* Fig. 15c) show variations with nozzle position consistent with the variations in lift increments.

To summarise, the tests at flaps 60 deg with a variable nozzle position have shown that the choice for the aircraft of a nozzle fixed in the flap nose, near to position 2 on the model, is satisfactory. Blowing from a nozzle further forward on the flap nose at, say, position 3, would be inferior, as would blowing from the wing shroud (which would be further forward still than position 3 at this flap angle). However, it would be dangerous to generalise on the relative merits of shroud-blowing and flap-blowing installations from the results obtained in one particular case; the comparison might well be different with other wing-flap configurations.

4.3. *Comparison between Blowing through Discrete Nozzles and Blowing through a Continuous Slit (Flaps 60 deg)*.—The arrangement of discrete circular nozzles shown in Fig. 2, having the same nozzle area as the conventional parallel slit, was tried at 60-deg flap deflection, position 2. At a given value of C_μ' and incidence (*see* Figs. 16a and 16d), the lift increment due to blowing was less than that produced with the normal slit configuration. The loss in lift amounted to $0\cdot14$, $0\cdot08$ at $C_\mu' = 0\cdot077$, $0\cdot154$ respectively. The loss decreased as C_μ' was increased (*cf.* the effect of nozzle position, Section 4.2) and might be acceptable at high values of C_μ'.

These tests show, as has been found in other tests with blowing over flaps, that quite large local variations in the spanwise distribution of C_μ' may be tolerable provided the overall distribution is uniform. The discrete nozzle arrangement tested, deliberately represented an extreme case; a more closely spaced arrangement of circular nozzles, such as might be used in practice, would probably behave almost as well as the usual parallel slit.

The drag curves (*see* Fig. 16b) are displaced by the use of the discrete nozzles, the drag rise associated with blowing being less than with the parallel slit. Presumably, the combined use of the discrete nozzles and the elevation of the jet above the flap surface resulted in a reduction in the effectiveness of the blowing.

The pitching-moment changes (*see* Fig. 16c) due to blowing are reduced for the discrete nozzle arrangement by an extent corresponding to the reduction in lift coefficient.

4.4. *Comparison between Blowing over the Outboard Flap only, and Blowing over Both Flaps.—Effect of Boom.*—As it was desirable to make comparisons between the measured and the estimated effects of blowing, it was necessary to understand the effects of the rather unusual combination of flaps and boom present on this aircraft. Tests were therefore made with blowing over the outboard flap only (with the inboard flap undeflected), in addition to the results obtained with both flaps deflected (Table 2). In addition, the boom was removed and the local wing trailing edge faired for brief tests with blowing over the outboard flap only with inboard flap undeflected; the results of these tests are given in Table 3.

In Figs. 17a to 17c, the results obtained with blowing over the outboard flap only are compared with the results obtained with blowing over both flaps (boom-on in each case). Note that the sectional momentum coefficient C_μ', quoted for the single-flap case corresponds to a smaller total jet momentum than at the same value of C_μ' with blowing over both flaps.

Fig. 17a shows the large effect of flap span on the lift increment due to the flap at constant C_μ' (including $C_\mu' = 0$). Fig. 17b shows the increased drag which occurs with the two part-span blown flaps. Fig. 17c shows the pitching-moment changes, which correspond to the lift effects. There appears to be a stability change in the tail-on case, which presumably results from the different downwash distributions of the two configurations.

Figs. 18a to 18c show the effect of removing the boom with only the outboard flap deflected. There is an appreciable loss in the flap lift increment produced by the blown flap when the boom is removed, which is thought to be due to the end-plate effect of the boom (*cf.* Section 4.9); with the unblown flap, the removal of the boom slightly increases the lift (again compare Section 4.9). There are only small effects on C_D vs. C_L (Fig. 18b) and the pitching-moment changes (Fig. 18c) are consistent with the changes in flap lift increment.

The lift increments produced at $\alpha = 5$ deg by blowing over both flaps (boom-on) and by blowing over the outboard flap only (boom-on and boom-off) are compared in Figs. 19a and 19b. In Fig. 19a, the comparison is made on the basis of the sectional momentum coefficient, C_{μ}'. It will be shown later (Section 5.1) that the observed variations in $\Delta C_{L\,(\mathrm{Flap}\,+\,\mathrm{Blow})}$ are consistent with the varying span of flap.

In Fig. 19b, the lift increments are compared, for this Figure only, using C_{μ}, the total momentum coefficient based on full wing area, S. Thus the comparison is now made on a constant engine-bleed basis. It will be seen that there is a large increase in $\Delta C_{L\,(\mathrm{Flap}\,+\,\mathrm{Blow})}$ as the total span of flap is increased. There is a small gain in $\Delta C_{L\,(\mathrm{Blow})}$ when the same jet momentum is applied to the larger span of flap, but the increase in $\Delta C_{L\,(\mathrm{Flap}\,+\,\mathrm{Blow})}$ is mainly due to the increase in the lift increment of the unblown configuration.

4.5. *The Effect of the Hook-Load Side Bar.*—The hook-load side bar (*see* Figs. 1 and 3), is an essential structural member between the boom and the fuselage, which transfers the load on the arrester hook to the fuselage. It forms part of the wing trailing edge in the flaps-up condition and remains stationary when the inboard flap is deflected, so that the latter is of trap-door type.

When blowing is applied to the inboard flap, the strong downwash at the hook-load bar produces a substantial negative lift increment which partially neutralises the additional flap lift. The effect of removing the hook-load bar was measured for a range of values for C_{μ}' at each flap angle; the results are given in Table 4 and illustrated by Fig. 20. It will be seen that removal of the bar resulted in gains in lift coefficient at constant incidence of up to $0 \cdot 06$. As there were corresponding pitching-moment increments of up to $-\ 0 \cdot 027$, the maximum gain in trimmed lift coefficient would be rather less than $0 \cdot 06$.

When a comparison is made between measured and estimated flap lift increments (Section 5.1), the comparison will be made for the model with hook-load side bar off. Comparison between the tunnel and the flight results will be made for the model with hook-load side bar on.

4.6. *The Effect of the Boom Flap.*—The boom flap is a curved metal plate spanning the boom and flush with the lower surface of the boom in the flaps-up case. It was intended to link the outboard and inboard flaps and would be deflected simultaneously with the flaps.

It was found (*see* Table 4) that the addition of the boom flap caused a lift loss with blown flaps, and it was consequently omitted in all subsequent tests. The results of Table 2 are quoted for the standard condition with boom flap off.

4.7. *The Effect of the Inboard-Flap Trailing-Edge Extension.*—It has been previously stated that the hook-load side bar occupied the wing trailing edge between the boom and the fuselage. In order to extend the chord of the inboard flap, a flat plate, which extended to the wing trailing edge, was bolted to the lower surface of the flap. This plate was flush with the hook-load side bar in the flaps-up condition (*see* Figs. 1 and 5).

Table 4 shows that this flap extension produced a small lift increment of the order $0 \cdot 01$, and the flap extension was consequently fitted to the inboard flap. The results quoted in Table 2 have all been presented for the standard condition with inboard flap extension on.

4.8. *The Effect of Applying Simulated Engine-Intake Flow.*—A representative series of repeat tests was made at 60-deg flaps, both with and without flap blowing, with suction applied to the engine intake to produce velocity ratios corresponding to approach and baulked-landing conditions. The air was led out from the model through a vertical flexible connection to a stirrup plate attached to the turn-table. This vertical pipe had to be ahead of the centre-line of rotation of the balance and the turn-table (*see* Fig. 1), and the connection from the stirrup plate to the suction pump had therefore to consist of a freely supported flexible pipe.

The only noticeable effect of the intake flow was found to be a drag increment* (*see* Table 4), which presumably resulted from the internal flow. There were no appreciable effects on C_L vs. α or C_m vs. C_L and the stalling behaviour was not affected. Therefore, for simplicity, the tests were mainly done with the intake faired over, and all results quoted in Tables 2 and 3 are given for this condition.

4.9. *The Effect of End-Plates.*—Small end-plates were fitted to the flaps, covering the areas swept out by the ends of the flaps as the flaps were deflected from 0 deg to the flap angle which was being tested. The effect of the end-plates is shown in Table 4 and Fig. 21.

At $C_\mu' = 0$, flaps 60 and 80 deg, the end-plates caused reductions in C_L of $-0 \cdot 023$ and $-0 \cdot 012$; at $C_\mu' = 0 \cdot 077$, the lift losses were only $-0 \cdot 009$ and $-0 \cdot 003$; and at $C_\mu' = 0 \cdot 154$, there were gains in C_L of $+0 \cdot 097$ and $+0 \cdot 034$ respectively.

Thus, at high values of C_μ', it might be worthwhile to fit such end-plates to increase further the lift increment resulting from blowing. It is thought that the end-plates may prevent spillage of the air jet over the ends of the flaps at high values of C_μ', and hence increase the efficiency of the blown flaps. Alternatively, it has been suggested that the end-plates produce an increase in the sectional lift slope over the flapped portion of the wing. This would appear to be unlikely to be the explanation, since one would then expect to obtain gains in the lift increment at all values of C_μ'.

The effect of the end-plate is very similar to the effect of the boom (*see* Section 4.4.)

The results quoted in Tables 2 and 3 are given for the model without end-plates. In the comparison given in Section 5.1 between measured and estimated lift increments, the measured increments are given for both end-plates on and end-plates off. In the flight-tunnel comparison, the tunnel results are given for end-plates off.

5. *Comparison between Estimated and Measured Effects of Blowing.*—5.1. *Comparison between Estimated and Measured No-Tail Values of $\Delta C_{L\,(\text{Flap + Blow})}$ at $\alpha = 5$ deg.*—Measured values of the flap lift increments at $\alpha = 5$ deg without tail are compared in Figs. 22a and 22b with estimated increments.

The estimated curves have been made using a method based on Refs. 4 to 9. The dashed curves were obtained by putting (*cf.* equation 4.1 of Ref. 4):

$$\text{Estimated } \Delta C_{L\,(\text{Flap + Blow})} = \frac{a_1}{2\pi} \times \lambda \times f(\beta) \times \frac{dC_L}{d\beta} \times \beta \quad \ldots \quad (1)$$

In this formula, β is the flap angle. The lift slope, a_1, would ideally be the mean sectional lift slope over that part of the wing spanned by the flaps. For the present case, with an unswept wing of moderately large aspect ratio, it seemed reasonable to use the theoretical lift slope corresponding to the aspect ratio of the wing (which agreed closely with the measured lift slopes). The part-span lift conversion factor, λ, was calculated from Ref. 5. Values of $dC_L/d\beta$, the theoretical flap effectiveness of a blown flap on a thin aerofoil at small deflection angles under two-dimensional conditions, have been taken from Fig. 1 of Ref. 6 for a range of values of the sectional momentum coefficient. It has been assumed that, at least in the case of an unswept wing of moderately high aspect ratio, the appropriate value for $dC_L/d\beta$ from Ref. 6 will be that value quoted at the same sectional momentum coefficient. (This approach may have to be modified for a swept wing configuration.) Finally, the linear theory of Ref. 6 does not allow for the theoretical reduction in the flap effectiveness of a flap in potential flow with increasing flap angle (Refs. 7 and 8), and it is therefore necessary to include a factor, $f(\beta)$, which is unity at zero flap deflection and progressively decreases with increasing flap angle, particularly for large chord flaps. Values for $f(\beta)$ estimated from Fig. 8 of Ref. 8 were $0 \cdot 936$, $0 \cdot 859$ and $0 \cdot 771$ at

* No allowance has been made in Table 4 for drag effects due to withdrawal of main-stream air from the model (*see* footnote to Section 4.1.2.).

flap angles of 40, 60 and 80 deg respectively. Thus, with 80-deg flaps, the linear theory would tend to over-estimate the theoretical flap lift increment by about 30 per cent for the 21 per cent chord flap here considered.

The values of ΔC_L obtained using equation (1) have been plotted as the dashed curves against sectional momentum coefficient, C_μ', in Figs. 22a and 22b. These curves are not realised in practice at low values of C_μ', as a result of separations, and the full curves shown were obtained as follows. Plain flap lift increments at $C_\mu' = 0$ were estimated in the normal way using the empirical method of Refs. 5 and 9, and the points thus obtained were connected to the dashed curves by characteristic S-shaped curves touching the dashed curves at values of C_μ' which increase steadily with flap angle ($C_\mu' = 0{\cdot}070$, $0{\cdot}154$, $0{\cdot}250$ at flap angles of 40, 60, 80 deg respectively). These values of C_μ' were taken from Fig. 11 of Ref. 4. At higher values of C_μ', the modified jet flap estimates by equation (1) have been used for the final estimated curves.

Fig. 22a shows the comparison between estimate and experiment for flap angles of 40, 60 and 80 deg with both flaps deflected. The experimental increments refer to the model with the hook-load side bar removed (*see* Section 4.5) and with blowing through the normal parallel slit at nozzle position 2. At flap deflection angles of 60 and 80 deg, the increments are also shown for the model with end plates attached to the flaps (*see* Section 4.9). The agreement between estimate and experiment is good for $C_\mu' > 0$ at 40 and at 60 deg; at 80 deg, the estimated lift increments were not fully attained on the model. In Section 5.2, it will be shown that this discrepancy may be associated with the high flap-induced drag which occurs with part-span blown flaps at large deflection angles.

Fig. 22b shows a similar comparison for the outboard flap only, with the inboard flap undeflected and the inboard nozzle sealed. In this case, one flap angle only (60 deg) was tested, with and without the tail boom (*see* Section 4.4). The presence of the boom increases the increments and the comparison with estimate should be made for the boom-off case. Similarly, in Fig. 22a, there is probably a somewhat larger favourable boom effect. This would decrease the lift increments for the blown flap given in Fig. 22a if allowance were made for the presence of the boom.

In all cases, the unblown lift increments are appreciably larger than estimate, and the method for estimating the total lift increments for the blown flap appears to be rather more satisfactory than the empirical methods available for estimating the lift increments produced by conventional unblown plain flaps. It is reasonable that this should be so, since the lift generated by a conventional flap may be affected greatly by the particular installation and local wing conditions, whereas, with a blown flap, the flow should be near potential and therefore the total lift generated by the flap should be more amenable to estimation. For this reason, it is advisable to estimate $\Delta C_{L\,(\mathrm{Flap\,+\,Blow})}$ directly, rather than try to estimate $\Delta C_{L\,(\mathrm{Flap})}$ for the unblown flap and $\Delta C_{L\,(\mathrm{Blow})}$ separately.

Thus, the method given here for estimating $\Delta C_{L\,(\mathrm{Flap\,+\,Blow})}$ at low-incidence values appears to give fairly close agreement at flap angles up to 60 deg. At 80 deg, the estimated increments for the blown flap were not fully attained, but it is thought that this (like the high drag increments), may be an induced effect associated with part-span blown flaps at large deflection angles (*see* Ref. 10).

5.2. *Comparison between Estimated and Measured No-Tail Values of* $[C_D - K/\pi A \,.\, C_L^2]$ *at low incidences*.—A comparison is made in Fig. 23 between measured no-tail values of $[C_D - K/\pi A \,.\, C_L^2]$ at low incidences (over the linear portions of the C_D vs. C_L^2 curves) and the corresponding estimated values. The estimates have been made in a conventional way by writing (*see* Ref. 10):

$$\left[C_D - \frac{K}{\pi A} C_L^2\right]_{\mathrm{estimated}} = C_{D\,0} + \nu \Delta C_{D\,0} + K'^2 \left(\Delta C_{L\,(\mathrm{Flap\,+\,Blow})}\right)^2 - C_\mu \cos\beta \quad \ldots \quad (2)$$

The symbols are defined in the Notation. Values of $C_{L\,(\mathrm{Flap\,+\,Blow})}$, C_μ, and the plain wing profile-drag coefficient, $C_{D\,0}$, were taken from the experimental results. The values of K', ν, and (in the unblown-flap case only) ΔC_{D0}, have been estimated using normal methods[5,9]. For the blown-flap case, the values for the sectional profile-drag coefficient, ΔC_{D0}, were estimated using the available two-dimensional data[11,12] on blown flaps (*see* Fig. 26).

It will be seen that agreement between measured and estimated values is satisfactory for the plain flap without blow. When blowing is applied to the flap, the estimated values are substantially lower than the measured values, particularly as the flap angle is increased. Moreover, the difference between estimated and measured values tends to become independent of C_μ once attached flow is attained over the flap (*see* also Ref. 10).

The values of $dC_D/d(C_L^2)$ over the linear portions of the C_D vs. C_L^2 curves are not affected substantially by blowing, so that the drag discrepancy is independent of C_L. The additional drag therefore acts as additional profile drag and tends to increase the absolute value of the minimum drag and to decrease the minimum-drag speed. Thus, this drag precludes the use of large deflection angles with part-span blown flaps at take-off, whilst the landing behaviour is improved as a result of the reduction in minimum-drag speed. This reduction in the minimum-drag speed is as important a consequence of flap blowing as the increased flap lift. In fact, it will not be possible on any aircraft to obtain the full advantage of the increased lift on the approach, unless the minimum-drag speed can be decreased by this or other means.

This discrepancy between estimated and measured drag has been found in other cases with small part-span blown flaps. Although an empirical method[10] has been devised to allow estimates to be made of the likely discrepancy in a particular case, further experimental and theoretical work is needed to develop a sound method for estimating the drag of an aircraft with part-span blown flaps.

5.3. *Comparison of Estimated and Measured No-Tail Values of* $(\Delta C_m/\Delta C_L)_{(\text{Flap + Blow})}$.—Fig. 24 shows measured no-tail values of $(\Delta C_m/\Delta C_L)_{(\text{Flap + Blow})}$ at $\alpha = 5$ deg plotted against C_μ'. The upper diagram gives results obtained with both flaps deflected and the hook-load side bar removed. The lower Figure gives results obtained with blowing over the outboard flap only, with inboard flap nozzle sealed. In this case, results are shown both with and without boom, which can be seen to have little effect.

The experimental values have been referred to mean quarter-chord position in this Figure. Theoretical values of $(\Delta C_m/\Delta C_L)$ about the quarter-chord point have been estimated from the revised version of Ref. 6 for a 21 per cent chord flap, allowing for the effect[9] of finite aspect ratio on ΔC_L. It will be seen that the agreement between experiment and theory is good, particularly at a flap angle of 40 deg. At higher angles, the experimental values were less negative than the estimated values. The predicted variation of $(\Delta C_m/\Delta C_L)$ with C_μ' was obtained.

It is probable that the values of $(\Delta C_m/\Delta C_L)_{(\text{Flap + Blow})}$ obtained under two-dimensional conditions could be used to make sufficiently accurate estimates for other unswept wings of moderately large aspect ratio with blown flaps.

As far as is known, there is no adequate method available for predicting the magnitude of the downwash changes at the tail due to blowing over a part-span flap and therefore no analysis has been attempted of the observed downwash effects at the tail.

6. *The Predicted Effect of Blowing over the Flaps on Approach and Take-off Speeds of the Modified Sea Venom Mk.* 21.—Stalling speeds have been predicted, from the values of trimmed maximum-lift coefficients measured in the tunnel for 40 and 60 deg flaps, at the normal take-off and landing weights of 15,000 and 12,000 lb respectively. Take-off and approach speeds have been calculated assuming:

$$\text{take-off speed} = 0\cdot 95V_s \text{ (rocket assisted take-off)}$$

$$\text{approach speed} = 1\cdot 25V_s$$

and are given in the following Table.

It should be noted that $C_{L\,max}$ should be larger at the full-scale Reynolds number (*see* Section 8.2) and this would lead to further reductions in approach and take-off speeds, although the relative performances of different configurations should be mainly unchanged. The values quoted in this Table have not been corrected for the effect of increased Reynolds number.

It may be found possible[13] to approach at the same incidence with blowing over the flap, as with the unblown flap. In that case the approach speed with flap blowing would be proportionately nearer to the stalling speed, and this would increase the differences between the approach speeds with and without blowing shown in the following Table.

Take-off (*A.U.W.* 15,000 *lb*)

Flaps (deg)	Bleed (per cent)	Trimmed $C_{L\,max}$	Stalling speed (kt)	Take-off speed (kt)
40	0	1·54	98	93
	7·7	1·82	90	86
	15·4	1·90	89	85

Approach (*A.U.W.* 12,000 *lb*)

Flaps (deg)	Bleed (per cent)	Approach trimmed C_L	Stalling speed (kt)	Approach speed (kt)
40	0	0·99	89	110
	11	1·17	81	101
60	0	0·98	89	111
	6·5	1·18	81	101
	11	1·23	78	98

From the above Tables, it would appear that a reduction of about ten knots in the approach speed should be obtained by the application of blowing to the flaps at 40 deg. The reduction achieved on the aircraft was of the same order. Further small reductions could be obtained at larger flap angles, although it should be realised that the drag would then be much larger in the case of a wave-off. This increased drag (*see* Section 7) would, however, be accompanied by decreases in the minimum-drag speeds. Also, the additional drag would permit the approach to be made at a higher throttle setting, and consequently at a higher value of C_μ'. Thus, the optimum flap angle for the approach will probably be a compromise and the value of 55 deg, based on the aircraft flight trials, seems to be reasonable.

7. *The Predicted Effect of Blowing on Minimum Drag and Minimum-Drag Speeds.*—It has been noted in Section 5.2, that the value of the drag coefficient at constant lift coefficient was increased substantially by blowing and, moreover, that the increase became progressively larger than estimate as the flap angle was increased. It was also shown that the additional drag tended to increase the minimum drag and decrease the minimum-drag speed.

Calculations based on the tunnel results gave, at 12,000 lb A.U.W., the following predicted minimum-drag speeds for the modified *Sea Venom* at approach conditions:

	Flaps 40 deg		Flaps 60 deg		Flaps 80 deg	
	No blow	With blow	No blow	With blow	No blow	With blow
Minimum drag speed (kt) ..	109	101	102	86	99	82
Minimum drag (lb)	1,660	1,760	1,940	2,480	2,130	3,030

8. *Flight/Tunnel Comparison.*—8.1. *Differences between the Model and the Aircraft Installation.*—The physical differences between the model and the subsequent aircraft installation are illustrated by Figs. 3 and 5, which show rear views of the flaps. On the aircraft (*see* Fig. 5), there was a flap gap and discontinuity in the wing upper-surface contour ahead of the flap, which could not be represented on the model because of the method of construction. Airflow through these gaps, or the discontinuity in contour, might have reduced the efficiency of the flap-blowing system on the aircraft. Apart from this gap, the inboard flap configurations were similar on model and aircraft.

Ahead of the inboard end of the outboard flap on the aircraft, there is a bulge in the upper-surface contour of the wing (*see* Fig. 5), which accommodates the undercarriage. This bulge was not represented on the model, since it was thought unlikely that it would have any large effects on the lift increments due to blowing. At the outboard end of the outboard flap, the aircraft installation proved to be difficult, and it was not found possible to extend blowing to the extreme end of the flap, where the nose of the flap was cut away. There was an additional break in the blowing nozzle on the outboard flap at about a quarter of the flap span from the outboard end of the flap (*see* Fig. 5). The influence of these two discontinuities on the effectiveness of the blown flap could be very large, particularly at large flap angles. Lastly, the nose of the flap had to be foreshortened over a considerable part of the outboard end of the flap, and the external appearance was restored by means of a cover plate. This cover plate (*see* Figs. 5 and 6) extended rearwards over the flap from the wing, to which it was attached. Consequently (*see* Fig. 6), as the flap angle was increased, it became progressively more difficult for the boundary layer to reattach to the flap.

In addition to the physical differences, the spanwise distributions of total head (and hence the momentum-coefficient distributions), showed much larger variations on the aircraft than on the model. This can be seen by comparing Figs. 7 and 8.

All these factors suggest that the effectiveness of the blown flap on the aircraft would be expected to be smaller than on the model, especially at large flap angles and this, in fact, was found to be the case (*see* next Section).

8.2. *Comparison between Lift Increments Measured on the Model and on the Aircraft.*—Fig. 25 shows for comparison trimmed values of $\Delta C_{L\,(\mathrm{Flap\,+\,Blow})}$ at $\alpha = 5$ deg, $\Delta C_{L\,\max\,(\mathrm{Blow})}$, and $C_{L\,\max}$ for the aircraft and the corresponding values measured on the tunnel model. The tunnel results are given for the standard condition with the hook-load side bar, and the inboard flap extension, on.

The mean flight values of trimmed flap lift increment for the unblown flap ($C_\mu' = 0$) are appreciably lower than the tunnel values. This could be due to the differences discussed in the previous Section. When blowing was applied at flaps 40 deg, the total lift increments, $\Delta C_{L\,(\mathrm{Flap\,+\,Blow})}$ at $\alpha = 5$ deg, obtained in the tunnel and on the aircraft show good agreement. Note that the values of $\Delta C_{L\,(\mathrm{Blow})}$ would not agree because of the differences in the values of the lift increments produced by the unblown flap.

At flap angles above 40 deg, the values of $\Delta C_{L\,(\mathrm{Flap\,+\,Blow})}$ obtained on the aircraft are considerably less than would be expected in view of the wind-tunnel curves. In flight, the optimum flap angle was 55 deg, above which the values of $\Delta C_{L\,(\mathrm{Flap\,+\,Blow})}$ started to decrease. This was in contrast to the results obtained in the tunnel, where the values of $\Delta C_{L\,(\mathrm{Flap\,+\,Blow})}$ continued to increase up to a flap angle of 80 deg. Tuft studies confirmed that flap blowing was less effective in suppressing the flap separations on the aircraft than on the model at the larger flap angles.

Thus, the blown flaps on the aircraft, whilst giving approximately the predicted lift increments at flaps 40 deg, failed to produce the expected further increases in lift increments when the flap angle was increased to higher values. This is what would be expected in view of the differences between the model and the aircraft geometry and blowing installation, and emphasises the desirability of representing all the peculiarities of the actual aircraft installation on the model (if these are known by the time the model is tested).

The trimmed values of $\Delta C_{L\max\,(\text{Blow})}$ obtained on the aircraft, although showing a large amount of scatter, again show the optimum flap angle for the aircraft to be 55 deg.

The flight/tunnel comparison indicates that there is a favourable Reynolds-number effect on trimmed $C_{L\max}$, which amounts to about $0 \cdot 10$ to $0 \cdot 15$ (no blow) and up to $0 \cdot 3$ (with blow). Thus the value of $\Delta C_{L\max\,(\text{Blow})}$ would seem to increase with Reynolds number. The values of $\Delta C_{L\,(\text{Blow})}$ at constant incidence below the stall are, however, unlikely to vary with Reynolds number.

9. *Conclusions*.—This report contains the results of low-speed tunnel tests of longitudinal stability on a modified *Sea Venom* Mk. 21 fitted with blowing over the flaps. At each flap angle, a range of values of the sectional momentum coefficient was tested. As a typical example, the increase in trimmed C_L at constant incidence resulting from blowing at flaps 60 deg was about $0 \cdot 45$, the increase in $C_{L\max}$ being somewhat smaller. The equivalent reduction in approach speed of 10 to 15 kt predicted from the tunnel results was later achieved in flight. The tunnel results suggested a beneficial reduction in minimum-drag speed due to blowing, particularly at large flap angles. Trim changes were large, amounting to about 8 deg on the all-movable tail at flaps 60 deg.

A comparison is made between estimated and measured effects of blowing. It is shown that, whilst the lift and pitching-moment increments resulting from flap blowing can be estimated fairly closely, the drag increments at large flap angles are much larger than would be expected. The additional drag tends to decrease the minimum-drag speed and increase the minimum drag, and may affect the take-off and landing performance appreciably. The effect will be unfavourable in the first case and favourable in the second.

A flight/tunnel comparison is included of the lift increments resulting from blowing. At flaps 40 deg, agreement is good, but at larger flap angles, the lift increments measured in flight were less than those measured on the model. Possible reasons for this are discussed. There is a favourable Reynolds-number effect on $C_{L\max}$ which is found to be somewhat larger for the blown flap than for the unblown flap.

NOTATION

a_1	Lift slope per radian
c	Local flap chord
c	Local wing chord
$\bar{c}$	Standard mean chord
$\bar{\bar{c}}$	Aerodynamic mean chord
C_D	Drag coefficient (including any jet thrust recovered)
C_{D0}	Plain wing profile-drag coefficient
C_L	Lift coefficient
C_m	Pitching-moment coefficient
ΔC_{D0}	Sectional profile-drag increment of unblown flap[5,9] or blown flap (Fig. 26)
$\Delta C_{L\,(\mathrm{Flap}+\mathrm{Blow})}$	Lift increment at $\alpha = 5$ deg due to flap + blow, referred to plain-wing C_L
$\Delta C_{L\,(\mathrm{Blow})}$	Lift increment at $\alpha = 5$ deg due to blow, referred to C_L at $C_\mu' = 0$ at the same flap angle
$\Delta C_{L\,\mathrm{max}\,(\mathrm{Flap}+\mathrm{Blow})}$	Increment in $C_{L\,\mathrm{max}}$ due to flap + blow, referred to plain-wing $C_{L\,\mathrm{max}}$
$\Delta C_{L\,\mathrm{max}\,(\mathrm{Blow}}$	Increment in $C_{L\,\mathrm{max}}$ due to blow, referred to $C_{L\,\mathrm{max}}$ at $C_\mu' = 0$ at the same flap angle
$\left(\dfrac{\Delta C_m}{\Delta C_L}\right)_{(\mathrm{Flap}+\mathrm{Blow})}$	Ratio of no-tail increments in C_m and C_L at $\alpha = 5$ deg, referred to plain-wing C_m and C_L
$C_\mu' = \dfrac{mv_j}{\frac{1}{2}\rho_0 U_0^2 S' g}$	Sectional momentum coefficient based on blown wing area
$C_\mu = \dfrac{mv_j}{\frac{1}{2}\rho_0 U_0^2 S g} = C_\mu' \dfrac{S'}{S}$	Momentum coefficient based on gross wing area
$\dfrac{dC_L}{d\beta}$	Theoretical flap effectiveness of a thin blown aerofoil at small flap deflection angles (Ref. 6)
$f(\beta)$	Theoretical reduction in flap effectiveness at large flap angles (Refs. 7 and 8)
K	$= \dfrac{dC_D}{d\left(\dfrac{C_L^2}{\pi A}\right)}$
K'^2	Constant used in estimate of flap-induced drag[5,9]: $C_{D\,i\,(\mathrm{Flap})} = K'^2(\Delta C_{L\,(\mathrm{Flap}+\mathrm{Blow})})^2$
m	Mass-flow rate (lb/sec)
p_D	Total head at nozzle (abs.)
p_0	Tunnel static pressure (abs.)

NOTATION—*continued*

v	Jet velocity after expansion to free-stream velocity
S	Wing area
S'	Blown wing area (*i.e.*, wing area spanned by flaps)
S''	Cross-sectional area of nozzle
T_D	Supply temperature, degrees absolute
U_0	Tunnel speed (ft/sec)
α	Wing incidence (deg)
β	Flap angle
ε	Downwash angle at tail (deg)
η_T	Tail setting angle (deg)
λ	Part-span lift conversion factor[5, 9]
ν	Part-span profile-drag conversion factor[5, 9]
ρ_0	Mainstream density
$\frac{1}{2}\rho_0 U_0^2$	Tunnel dynamic head, expressed in lb/sq ft in the momentum formulae

REFERENCES

No.	Author	Title, etc.
1	S. F. J. Butler and M. B. Guyett ..	Preliminary note on wind tunnel tests on the De Havilland *Sea Venom* with blowing over the flaps. R.A.E. Tech. Note Aero. 2431. A.R.C. 18,563. November, 1955.
2	A. Anscombe and J. Williams ..	Some comments on high-lift testing in wind tunnels with particular reference to jet-blowing models. R.A.E. Tech. Note Aero. 2460. A.R.C. 18,664. A.G.A.R.D. Report No. 63. June, 1956.
3	E. C. Maskell	Theory of wind-tunnel blockage effects on stalled flows. R.A.E. Report. (To be issued.)
4	J. Williams	An analysis of aerodynamic data on blowing over trailing-edge flaps for increasing lift. C.P. 209. September, 1954.
5	——	Royal Aeronautical Society Aerodynamic Data Sheets.
6	D. A. Spence	The lift on a thin aerofoil with a blown flap. R.A.E. Tech. Note Aero. 2450. A.R.C. 18,473. May, 1956.
	A. J. Ross and D. A. Spence ..	The pitching moment on a thin aerofoil with a blown flap. Addendum to R.A.E. Tech. Note Aero. 2450. June, 1958.
7	F. Keune	Auftrieb einer geknickten ebenen Platte. *L.F.F.* Vol. 13. 1936. (Translated in N.A.C.A. Tech. Memo. 1340.)
8	J. A. Hay and W. J. Eggington ..	An exact theory of a thin aerofoil with large flap deflection. Aerodynamics Department Report. Vickers-Armstrong (Aircraft), Limited. April, 1956.
9	A. D. Young	The aerodynamic characteristics of flaps. R. & M. 2622. February, 1947.
10	S. F. J. Butler	The drag increments associated with part-span blown flaps. R.A.E. (Unpublished paper.)
11	E. L. Harkleroad and R. D. Murphy	Two-dimensional wind-tunnel tests of a model of a F9F–5 airplane wing section using a high-speed jet blowing over a flap. Part I. Tests of a 6-ft model. U.S.A. David Taylor Model Basin Aero. Report 845. May, 1953.
12	R. R. Jessop, J. R. Wedderspoon and A. C. G. Seal	Two-dimensional tests on a flapped *Viscount* aerofoil employing boundary-layer control by means of blowing. Vickers-Armstrong Wind-Tunnel Report 2113. Part II.
13	G. E. Cooper and R. C. Innis ..	Effect of area-suction-type boundary-layer control on the landing-approach characteristics of a 35-deg swept-wing fighter. N.A.C.A. Research Memo. A55K14. NACA/TIL 4952. February, 1956.

(75640) B

TABLE 1

Model Data

All dimensions model scale (2/7th-scale model)

Wing (one wing only)	
Area (projected) S	12·07 sq ft
Semi-span (excluding tip tank) $\frac{1}{2}b$	5·48 ft
Standard mean chord $\bar{c}$	2·20 ft
Aerodynamic mean chord $\bar{\bar{c}}$	2·34 ft
$\bar{c}/\bar{\bar{c}}$	0·939
Aspect ratio (full span) A	4·98
Section (Modified by 1·98 per cent drooped leading-edge extension)	EQ.1040
Wing thickness/chord ratio	0·095
Centre-line wing chord (projected)	3·10 ft
Tip chord	1·25 ft
Sweepback of leading edge	17° 40′
Dihedral	3°
Wing-fuselage angle	0°
Taper ratio (centre-line chord/tip chord)	2·48
Flaps	
Area of half wing to which trailing-edge flaps are applied S'	5·00 sq ft
Average value of c_f/c (aft of hinge line)	0·21
Spanwise extent of flaps, measured from fuselage centre-line:	
Outboard flap	$0·567b/2$ to $0·287b/2$
Inboard flap	$0·217b/2$ to $0·119b/2$
Tailplane (half tailplane only)	
Area S_t	1·44 sq ft
Semi-span $\frac{1}{2}b_t$	1·32 ft
Standard mean chord $\bar{c}_t$	1·09 ft
Aerodynamic mean chord $\bar{\bar{c}}_t$	1·09 ft
Aspect ratio (full span) A_t	2·42
Height of centre-line of tailplane:	
Above c.g. position	0·70 ft
Above centre-line wing chord	0·74 ft
Arm (c.g. position to mean quarter-chord point of tail) l_t	4·85 ft
Volume coefficient $\bar{v} = \dfrac{S_t l_t}{S\bar{\bar{c}}}$	0·248
Sweepback	0°
Dihedral	0°
Taper ratio	1·00
C.g. position	
Above centre-line wing chord	0·043 ft
Aft of transverse datum	0·296 ft
Aft of projected wing apex	1·411 ft
Aft of leading edge of standard mean chord	$0·285\bar{c}$
Aft of leading edge of aerodynamic mean chord	$0·283\bar{\bar{c}}$

TABLE 2

Lift, Drag and Pitching-Moment Coefficients with Standard Aircraft Configuration

The results in this Table are quoted for the standard model condition:

Boom on
Inboard flap extension on
Hook-load bar on
Engine intake faired
Boom flap off
End plates off.

Results obtained with the boom removed and local wing trailing edge faired are given in Table 3. The effect of various other modifications to the standard condition are given in Table 4.

(*a*) *Flaps Up*

Nozzle position	C_μ'*	Tail	α deg	C_L	C_D	C_m
—	0	Tail off	− 0·05	−0·053	+0·020	+0·002
			+ 4·28	+0·287	0·025	0·022
			8·63	0·638	0·0495	0·035
			12·96	0·977	0·094	0·048
			15·10	1·115	0·121	0·053
			17·16	1·187	0·181	+0·045
			+17·91	+0·931	+0·2505	−0·022
		$\eta_T = -3°$	− 0·05	−0·078	+0·0215	+0·0445
			+ 4·28	+0·274	0·026	0·039
			8·63	0·642	0·0515	0·0245
			12·96	0·996	0·097	0·0065
			15·10	1·141	0·127	+0·003
			16·22	1·180	0·1595	−0·0055
			17·16	1·213	0·188	−0·0125
			+17·91	+0·957	+0·2605	−0·0665
		$\eta_T = -6·1°$	− 0·05	−0·097	+0·0225	+0·089
			+ 4·28	+0·257	0·0255	0·079
			8·63	0·623	0·050	0·067
			+15·09	+1·123	+0·1225	+0·046
1	0·070	Tail off	− 0·02	−0·020	0	−0·008
			+ 4·32	+0·329	+0·0075	+0·009
			8·67	0·692	0·0365	0·019
			13·02	1·043	0·085	0·0275
			16·21	1·236	0·146	0·029
			17·24	1·272	0·175	0·027
			+17·97	+0·992	+0·2505	+0·040
		$\eta_T = -3°$	− 0·02	−0·052	+0·001	+0·0375
			+ 4·31	+0·311	0·007	0·0315
			+ 8·67	+0·690	+0·0365	+0·018

* C_μ' is based on the flapped area of the wing, S', and is therefore the mean sectional momentum coefficient.

TABLE 2—*continued*

(*b*) *Flaps* 40 *deg*

Nozzle position	C_μ'	Tail	α deg	C_L	C_D	C_m
—	0	Tail off	+ 0·39	+0·393	+0·0865	−0·068
			4·71	0·728	0·1095	−0·0515
			9·03	1·051	0·1455	−0·0355
			13·31	1·347	0·1965	−0·017
			16·48	1·530	0·2675	−0·0115
			17·50	1·539	0·2995	−0·0145
			+18·00	+1·026	+0·3535	−0·090
		$\eta_T = -3°$	+ 0·39	+0·351	+0·0875	+0·0075
			4·71	0·700	0·110	+0·0005
			9·03	1·041	0·1455	−0·007
			13·31	1·356	0·197	−0·017
			16·48	1·532	0·2705	−0·0325
			17·50	1·558	0·3035	−0·0395
			+18·00	+1·043	+0·3565	−0·107
		$\eta_T = -6·1°$	+ 0·39	+0·333	+0·0895	+0·050
			4·71	0·679	0·110	0·0415
			9·03	1·022	0·145	0·0315
			13·31	1·336	0·195	0·023
			+16·48	+1·514	+0·268	+0·009
1	0·077	Tail off	+ 0·73	+0·746	+0·121	−0·141
			5·09	1·108	0·166	−0·1305
			9·42	1·451	0·226	−0·1195
			13·72	1·764	0·3035	−0·106
			16·80	1·847	0·359	−0·0905
			+17·17	+1·197	+0·357	−0·083
		$\eta_T = -3°$	+ 0·73	+0·708	+0·123	−0·061
			5·09	1·081	0·1665	−0·073
			9·42	1·445	0·227	−0·084
			13·72	1·762	0·305	−0·0945
			16·80	1·857	0·361	−0·090
			+17·17	+1·205	+0·3625	−0·086
	0·154	Tail off	+ 0·78	+0·792	+0·1145	−0·1595
			5·13	1·157	0·1625	−0·147
			9·48	1·507	0·2265	−0·1345
			13·77	1·815	0·3085	−0·120
			+16·89	+1·934	+0·3745	−0·1035
		$\eta_T = -3°$	+ 0·78	+0·744	+0·1135	−0·0735
			5·13	1·122	0·161	−0·083
			9·48	1·483	0·2245	−0·095
			13·77	1·818	0·309	−0·107
			+16·89	+1·932	+0·3765	−0·122

TABLE 2—*continued*

(*b*) *Flaps* 40 *deg—continued*

Nozzle position	C_{μ}'	Tail	α deg	C_L	C_D	C_m
2	0·077	Tail off	+ 0·72	+0·739	+0·1185	−0·140
			5·07	1·101	0·1625	−0·1295
			9·42	1·445	0·2215	−0·1175
			13·71	1·752	0·2955	−0·1005
			16·81	1·849	0·350	−0·078
			+17·78	+1·812	+0·358	−0·0645
		$\eta_T = -3°$	+ 0·72	+0·693	+0·119	−0·0595
			5·07	1·069	0·1625	−0·0715
			9·42	1·429	0·2215	−0·0835
			13·71	1·756	0·2965	−0·093
			16·81	1·868	0·352	−0·0885
			+17·78	+1·842	+0·362	−0·0835
		$\eta_T = -6·1°$	+ 0·72	+0·676	+0·118	−0·021
			5·07	1·052	0·161	−0·0325
			9·42	1·413	0·2195	−0·0445
			13·71	1·739	0·295	−0·0535
			+16·81	+1·845	+0·3505	−0·0475
	0·154	Tail off	+ 0·78	+0·803	+0·1095	−0·1575
			5·15	1·168	0·1595	−0·149
			9·49	1·522	0·2245	−0·148
			13·77	1·811	0·306	−0·129
			16·91	1·950	0·3755	−0·1135
			+17·22	+1·249	+0·3685	−0·1015
		$\eta_T = -3°$	+ 0·78	+0·753	+0·1105	−0·0755
			5·15	1·132	0·1575	−0·0865
			9·49	1·500	0·2215	−0·0945
			13·77	1·837	0·3055	−0·107
			16·91	1·953	0·3765	−0·113
			+17·22	+1·240	+0·3605	−0·104
		$\eta_T = -6·1°$	+ 0·78	+0·733	+0·1115	−0·0345
			5·15	1·110	0·1595	−0·0485
			9·49	1·470	0·223	−0·061
			13·77	1·798	0·3055	−0·0715
			16·91	1·944	0·376	−0·074
			17·21	1·379	0·350	−0·0395
			+18·19	+1·235	+0·378	−0·0815

TABLE 2—*continued*

(*c*) *Flaps* 60 *deg*

Nozzle position	C_{μ}'	Tail	α deg	C_L	C_D	C_m
—	0	Tail off	+0·45	+0·516	+0·128	−0·074
			4·75	0·830	0·1525	−0·0595
			9·06	1·140	0·1915	−0·046
			13·34	1·426	0·2455	−0·029
			14·37	1·466	0·258	−0·023
			15·42	1·506	0·2775	−0·0175
			16·44	1·535	0·304	−0·016
			+16·95	+1·028	+0·3725	−0·092
		$\eta_T = 0°$	+0·58	+0·505	+0·1255	−0·0305
			4·94	0·835	0·150	−0·0395
			9·19	1·158	0·190	−0·049
			13·48	1·466	0·2475	−0·0595
			13·59	1·476	0·2505	−0·0595
			15·66	1·564	0·292	−0·061
			+16·22	+1·092	+0·375	−0·117
		$\eta_T = -3°$	+0·50	+0·469	+0·1275	+0·002
			4·80	0·801	0·1505	−0·008
			9·10	1·126	0·190	−0·0175
			11·23	1·280	0·2145	−0·0225
			13·39	1·429	0·2455	−0·0275
			14·42	1·472	0·2575	−0·0285
			15·47	1·518	0·2795	−0·031
			16·49	1·556	0·307	−0·035
			+17·00	+1·027	+0·3715	−0·106
		$\eta_T = -6·1°$	+0·50	+0·442	+0·1285	+0·045
			9·10	1·098	0·1865	0·024
			15·47	1·502	0·2745	0·0135
			+16·50	+1·536	+0·302	+0·0085
1	0·046	Tail off	+0·92	+0·958	+0·232	−0·1655
			5·25	1·282	0·2775	−0·1565
			9·54	1·577	0·3295	−0·141
			11·68	1·717	0·3615	−0·1315
			13·78	1·815	0·388	−0·1175
			14·80	1·842	0·399	−0·1085
			15·80	1·851	0·4065	−0·095
			16·65	1·696	0·353	−0·0515
			+17·15	+1·178	+0·379	−0·0805
		$\eta_T = 0°$	+1·14	+0·959	+0·2365	−0·1015
			5·46	1·299	0·2875	−0·1125
			9·77	1·614	0·3365	−0·1215
			14·00	1·867	0·401	−0·1285
			15·01	1·892	0·407	−0·127
			16·04	1·906	0·4075	−0·145
			+16·31	+1·131	+0·379	−0·127

TABLE 2—*continued*

(*c*) *Flaps* 60 *deg—continued*

Nozzle position	C_μ'	Tail	α deg	C_L	C_D	C_m
1	0·046	$\eta_T = -3°$	+ 0·92	+0·897	+0·231	−0·070
			5·25	1·237	0·275	−0·0795
			9·54	1·554	0·3265	−0·090
			11·68	1 699	0·356	−0·094
			13·78	1·822	0·383	−0·0965
			14·80	1·840	0·397	−0·0955
			15·80	1·854	0·406	−0·088
			16·65	1·712	0·3455	−0·049
			+17·15	+1·093	+0·381	−0·111
	0·077	Tail off	+ 0·98	+1·005	+0·2475	−0·179
			5·29	1·331	0·294	−0·168
			9·60	1·641	0·359	−0·1535
			11·74	1·786	0·387	−0·1445
			13·84	1·888	0·4185	−0·1335
			14·88	1·927	0·4335	−0·125
			15·89	1·939	0·444	−0·113
			16·88	1·925	0·434	−0·098
			+17·07	+1·101	+0·395	−0·111
		$\eta_T = -3°$	+ 0·98	+0·944	+0·2475	−0·0795
			5·29	1·285	0·294	−0·092
			9·60	1·601	0·352	−0·101
			11·74	1·763	0·385	−0·1045
			13·84	1·887	0·420	−0·105
			14·88	1·922	0·4315	−0·103
			15·89	1·923	0·4415	−0·0955
			16·88	1·905	0·4335	−0·0885
			+17·07	+1·206	+0·382	−0·1205
2	0·046	Tail off	+ 0·92	+0·949	+0·226	−0·1615
			5·25	1·279	0·270	−0·150
			9·54	1·584	0·322	−0·134
			11·68	1·718	0·3505	−0·1245
			13·80	1·838	0·380	−0·112
			15·83	1·884	0·403	−0·092
			16·81	1·859	0·3965	−0·074
			+17·03	+1·064	+0·368	−0·095
		$\eta_T = -3°$	+ 0·92	+0·887	+0·225	−0·0695
			5·25	1·237	0·2685	−0·0795
			9·54	1·549	0·3185	−0·087
			11·68	1·696	0·348	−0·0895
			13·80	1·829	0·379	−0·0905
			15·83	1·873	0·4025	−0·084
			16·81	1·856	0·3955	−0·073
			+17·03	+1·074	+0·372	−0·1075

TABLE 2—*continued*

(*c*) *Flaps* 60 *deg—continued*

Nozzle position	C_μ'	Tail	α deg	C_L	C_D	C_m
2	0·046	$\eta_T = -6\cdot1°$	+ 0·92 5·25 9·54 13·80 +16·81	+0·871 1·219 1·529 1·805 +1·752	+0·229 0·269 0·3185 0·377 +0·393	−0·036 −0·041 −0·0505 −0·0535 −0·0335
	0·077	Tail off	+ 0·98 5·32 9·61 11·75 13·87 15·92 16·93 +17·07	+1·015 1·354 1·656 1·798 1·919 1·969 1·956 +1·108	+0·2455 0·292 0·349 0·382 0·417 0·4425 0·437 +0·371	−0·1785 −0·166 −0·1525 −0·143 −0·131 −0·1125 −0·098 −0·104
		$\eta_T = -3°$	+ 0·98 5·32 9·61 11·75 13·87 15·92 16·93 +17·07	+0·961 1·303 1·623 1·776 1·903 1·957 1·950 +1·103	+0·243 0·290 0·3475 0·3795 0·414 0·441 0·4365 +0·3725	−0·082 −0·0915 −0·101 −0·1025 −0·1025 −0·0975 −0·0885 −0·1065
		$\eta_T = -6\cdot1°$	+ 0·98 9·61 13·87 +16·91	+0·943 1·610 1·890 +1·930	+0·247 0·3475 0·4145 +0·437	−0·051 −0·0645 −0·0665 −0·050
	0·132	Tail off	+ 1·05 +13·93	+1·084 +1·981	+0·2595 +0·4495	−0·193 −0·1495
		$\eta_T = -3°$	+ 1·05 +13·93	+1·024 +1·971	+0·2585 +0·448	−0·0935 −0·118
	0·154	Tail off	+ 1·08 9·71 13·97 +16·52	+1·101 1·751 2·014 +2·068	+0·257 0·375 0·4515 +0·4835	−0·1975 −0·174 −0·154 −0·132
		$\eta_T = -3°$	+ 1·08 9·71 +13·97	+1·044 1·716 +1·996	+0·259 0·3745 +0·4515	−0·100 −0·116 −0·1175
	0·264	Tail off	+ 1·20 +14·10	+1·188 +2·091	+0·260 +0·488	−0·2275 −0·1785

TABLE 2—*continued*

(*c*) *Flaps* 60 *deg—continued*

Nozzle position	C_μ'	Tail	α deg	C_L	C_D	C_m
3	0·046	Tail off	+ 0·83	+0·840	+0·1995	−0·141
			9·41	1·445	0·2805	−0·1075
			15·75	1·786	0·363	−0·0715
			16·76	1·803	0·3805	−0·065
			+17·08	+1·111	+0·3765	−0·098
		$\eta_T = -3°$	+ 0·83	+0·788	+0·1995	−0·0545
			9·41	1·421	0·279	−0·069
			15·75	1·773	0·3635	−0·071
			16·76	1·800	0·3765	−0·0515
			+17·08	+1·107	+0·3825	−0·110
	0·077	Tail off	+ 0·96	+0·995	+0·2405	−0·175
			9·59	1·635	0·344	−0·1475
			15·90	1·954	0·4375	−0·110
			16·90	1·952	0·4375	−0·0955
			+17·10	+1·129	+0·381	−0·1105
		$\eta_T = -3°$	+ 0·96	+0·945	+0·2385	−0·0805
			9·59	1·604	0·3435	−0·101
			15·88	1·930	0·442	−0·099
			+16·89	+1·945	+0·439	−0·095

(*d*) *Flaps* 80 *deg*

Nozzle position	C_μ'	Tail	α deg	C_L	C_D	C_m
—	0	Tail off	+ 0·56	+0·556	+0·145	−0·058
			4·87	0·870	0·1695	−0·0435
			9·13	1·172	0·2055	−0·028
			13·44	1·443	0·260	−0·0085
			16·56	1·547	0·3225	+0·0025
			+17·13	+1·046	+0·398	−0·0745
		$\eta_T = -3°$	+ 0·56	+0·510	+0·146	+0·021
			4·87	0·840	0·169	0·0125
			9·13	1·154	0·205	+0·0055
			13·44	1·439	0·2605	−0·001
			15·50	1·533	0·298	−0·005
			16·56	1·554	0·324	−0·006
			+17·13	+1·062	+0·398	−0·0825

TABLE 2—*continued*

(*d*) *Flaps* 80 *deg—continued*

Nozzle position	C_μ'	Tail	α deg	C_L	C_D	C_m
2	0·077	Tail off	+ 1·11	+1·135	+0·3405	−0·1805
			5·40	1·436	0·380	−0·164
			9·68	1·722	0·434	−0·1455
			13·91	1·953	0·495	−0·1205
			14·60	1·647	0·332	−0·040
			15·65	1·686	0·352	−0·0345
			16·69	1·720	0·375	−0·0325
			+17·11	+1·130	+0·4185	−0·0915
		$\eta_T = -3°$	+ 1·10	+1·082	+0·3435	−0·0775
			5·40	1·401	0·3825	−0·075
			9·68	1·702	0·4325	−0·088
			13·91	1·937	0·492	−0·0875
			+14·60	+1·635	+0·4335	−0·0195
	0·154	Tail off	+ 1·22	+1·259	+0·3925	−0·2065
			5·53	1·565	0·440	−0·1915
			9·82	1·860	0·5025	−0·174
			14·03	2·072	0·5685	−0·1485
			15·03	2·075	0·5725	−0·1345
			16·04	2·084	0·570	−0·125
			16·18	1·210	0·4375	−0·1145
			+17·17	+1·197	+0·457	−0·1105
		$\eta_T = -3°$	+ 1·22	+1·198	+0·3885	−0·099
			5·53	1·498	0·4345	−0·1025
			9·82	1·822	0·495	−0·1075
			14·03	2·052	0·558	−0·1085
			15·03	2·050	0·5615	−0·1005
			16·04	2·078	0·5595	−0·0975
			+16·18	+1·220	+0·4365	−0·115

(*e*) *Flaps* 60 *deg*

Blowing Through Discrete Nozzles

Nozzle position	C_μ'	Tail	α deg	C_L	C_D	C_m
2	0	Tail off	+ 0·49	+0·495	+0·1205	−0·0685
			9·10	1·126	0·183	−0·0395
			+16·50	+1·522	+0·300	−0·009
		$\eta_T = -3°$	+ 0·49	+0·447	+0·121	+0·008
			9·10	1·112	0·1825	−0·009
			+16·50	+1·549	+0·3025	−0·0225

TABLE 2—*continued*

(*e*) *Flaps* 60 *deg—continued*

Nozzle position	C_μ'	Tail	α deg	C_L	C_D	C_m
2	0·077	Tail off	+ 0·87	+0·882	+0·206	−0·151
			5·17	1·202	0·2445	−0·1365
			9·47	1·501	0·2905	−0·1185
			13·74	1·770	0·3535	−0·0985
			16·83	1·869	0·406	−0·081
			+17·12	+1·139	+0·4005	−0·1075
		$\eta_T = -3°$	+ 0·87	+0·842	+0·2075	−0·0615
			9·47	1·492	0·293	−0·073
			+16·83	+1·894	+0·4135	−0·079
	0·154	Tail off	+ 0·98	+1·012	+0·233	−0·185
			9·63	1·655	0·3435	−0·156
			16·47	2·011	0·466	−0·1235
			+16·24	+1·275	+0·407	−0·134
		$\eta_T = -3°$	+ 0·98	+0·967	+0·233	−0·085
			9·63	1·637	0·342	−0·1045
			+16·47	+2·007	+0·4645	−0·106

(*f*) *Outboard Flap* 60 *deg: Inboard Flap Undeflected*

Blowing over Outboard Flap only

Nozzle position	C_μ'*	Tail	α deg	C_L	C_D	C_m
—	0	Tail off	+ 0·35	+0·367	+0·0795	−0·062
			4·68	0·697	0·101	−0·0455
			9·00	1·024	0·1395	−0·0305
			13·30	1·325	0·1945	−0·0135
			16·45	1·478	0·254	−0·003
			17·47	1·497	0·2825	−0·0025
			+18·13	+1·149	+0·3025	+0·0005
		$\eta_T = -3°$	+ 0·35	+0·336	+0·0805	−0·0009
			4·68	0·679	0·1005	−0·018
			9·00	1·022	0·1395	−0·0335
			13·30	1·342	0·1955	−0·047
			16·45	1·502	0·258	−0·0515
			17·47	1·523	0·288	−0·054
			+18·13	+1·028	+0·363	−0·1175

* C_μ' is now expressed in terms of the reduced S' corresponding to the outboard flap only.

TABLE 2—*continued*

(f) Outboard Flap 60 *deg: Inboard Flap Undeflected—continued*

Nozzle position	C_μ'	Tail	α deg	C_L	C_D	C_m
2	0·080	Tail off	+ 0·77	+0·781	+0·1765	−0·1545
			5·11	1·157	0·2295	−0·149
			9·45	1·486	0·288	−0·1365
			13·74	1·779	0·3595	−0·117
			16·81	1·853	0·3945	−0·0875
			+17·22	+1·253	+0·3185	−0·0385
		$\eta_T = -3°$	+ 0·77	+0·740	+0·178	−0·0815
			5·11	1·128	0·230	−0·101
			9·45	1·477	0·288	−0·116
			13·74	1·788	0·361	−0·1255
			16·81	1·874	0·397	−0·129
			+17·22	+1·098	+0·365	−0·1185
	0·160	Tail off	+ 0·81	+0·834	+0·188	−0·172
			5·18	1·212	0·2445	−0·167
			9·51	1·545	0·307	−0·155
			13·80	1·840	0·3835	−0·1375
			16·88	1·932	0·4365	−0·112
			+17·47	+1·513	+0·3765	−0·065
		$\eta_T = -3°$	+ 0·81	+0·818	+0·1895	−0·0945
			5·18	1·186	0·245	−0·114
			9·51	1·532	0·3075	−0·128
			13·80	1·853	0·386	−0·134
			16·88	1·954	0·4345	−0·1435
			+17·38	+1·165	+0·3815	−0·129

TABLE 3

Lift, Drag and Pitching-Moment Coefficients with Boom Removed and Wing Trailing Edge Faired

(a) Flaps up

Nozzle position	C_μ'	Tail	α deg	C_L	C_D	C_m
—	0	Off	−0·04 +4·30 +8·64	−0·034 +0·303 +0·647	+0·0165 0·023 +0·049	+0·0015 0·0225 +0·036

(b) Outboard flap 60 deg: Inboard Flap Undeflected Blowing over Outboard Flap only

Nozzle position	C_μ'*	Tail	α deg	C_L	C_D	C_m
—	0	Off	+0·39 4·50 +9·03	+0·399 0·727 +1·051	+0·0775 0·0995 +0·1395	−0·0665 −0·0485 −0·031
2	0·080	Off	+0·71 5·06 +9·38	+0·724 1·087 +1·418	+0·1665 0·215 +0·271	−0·138 −0·1285 −0·114
	0·160	Off	+0·76 5·11 +9·44	+0·779 1·139 +1·478	+0·1765 0·228 +0·2875	−0·1535 −0·145 −0·131

* C_μ' in terms of the reduced S' corresponding to the outboard flap only.

TABLE 4

Effect of Various Modifications to the Standard Test Configuration

The results in Table 2 are quoted for the model condition:

Inboard flap extension on

Hook-load bar on

Engine-intake faired

Boom flap off

End plates off.

The effects of these components at constant incidence are listed in the following Tables:

The effect of removing inboard-flap trailing-edge extension

Flap angle (deg)	C_{μ}'	ΔC_L	ΔC_D	ΔC_m
40	0	−0·010	−0·005	0
60	0·077	−0·005	−0·003	0

The effect of removing hook-load bar

Flap angle (deg)	C_{μ}'	ΔC_L	ΔC_D	ΔC_m
40	0	0	0	−0·005
	0·007	+0·060	+0·008	−0·016
	0·154	+0·060	+0·010	−0·027
60	0	+0·010	0	−0·007
	0·077	0·040	+0·007	−0·014
	0·154	+0·050	+0·015	−0·020
80	0	+0·010	0	−0·004
	0·077	0·030	−0·006	−0·011
	0·154	+0·030	−0·006	−0·011

The effect of applying suction through engine intake

Air intake velocity ratio	ΔC_L	ΔC_D	ΔC_m
Normal approach . .	0	+0·030	0
Baulked landing. . . .	0	+0·041	0

TABLE 4—*continued*

The effect of adding boom flap

Flap angle (deg)	C_{μ}'	ΔC_L	ΔC_D	ΔC_m
60	0·077	−0·030	−0·002	+0·014

The effect of adding end-plates to both flaps

Flap angle (deg)	C_{μ}'	ΔC_L	ΔC_D	ΔC_m
60	0 0·077 0·154	−0·023 −0·009 +0·097	−0·004 −0·009 +0·013	+0·001 −0·002 −0·027
80	0 0·077 0·154	−0·012 −0·003 +0·034	−0·002 −0·010 0	+0·002 −0·002 −0·009

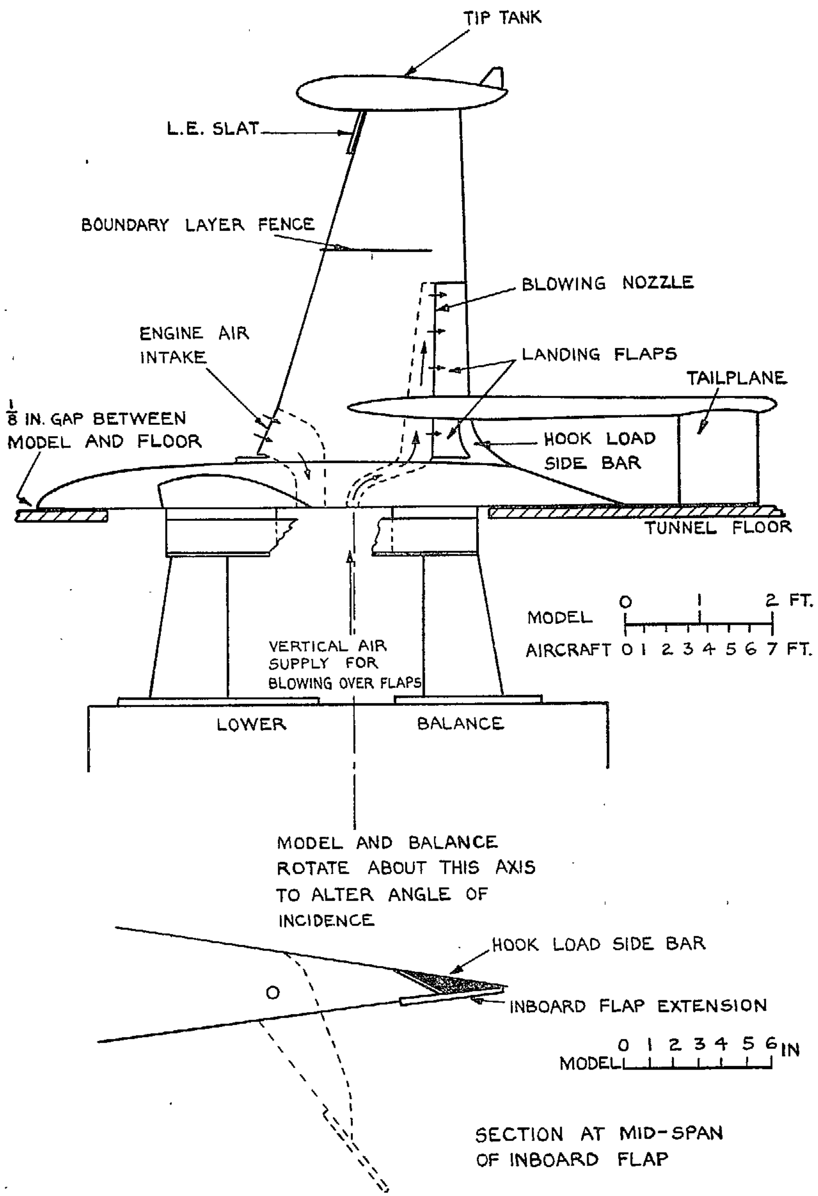

FIG. 1. Model installation.

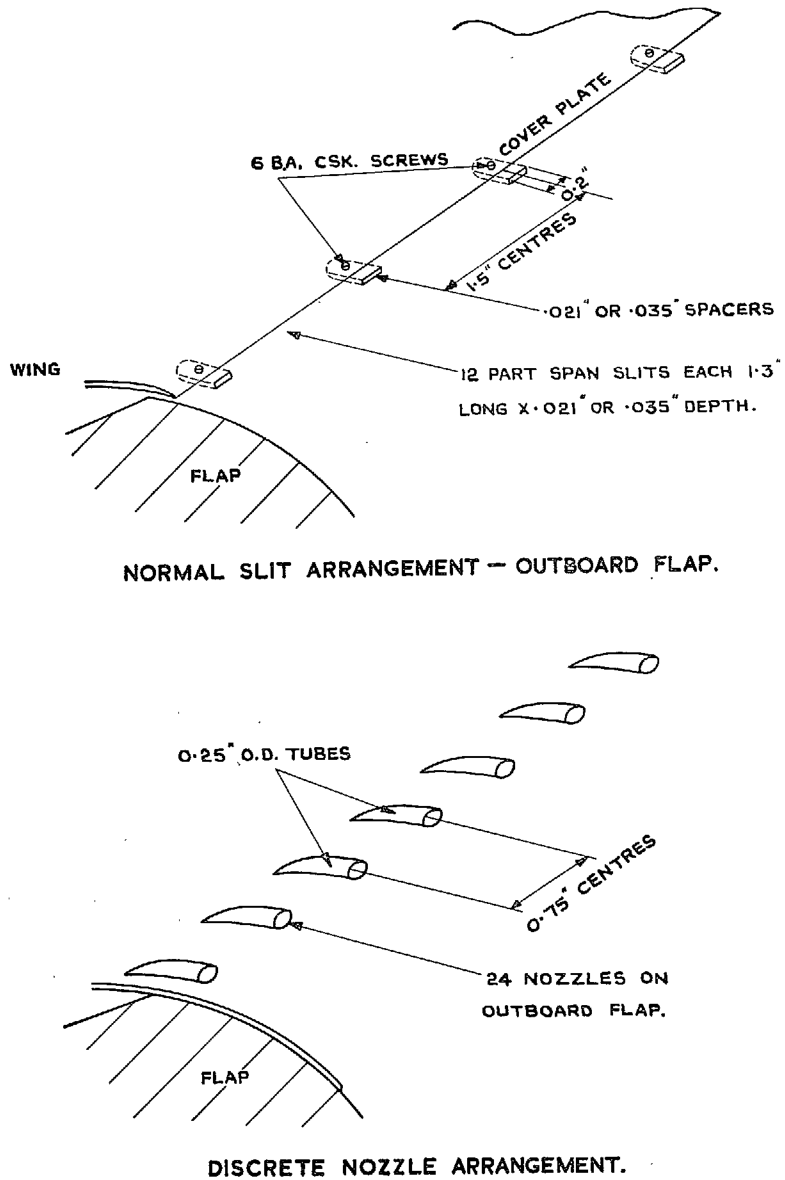

FIG. 2. Details of nozzles.

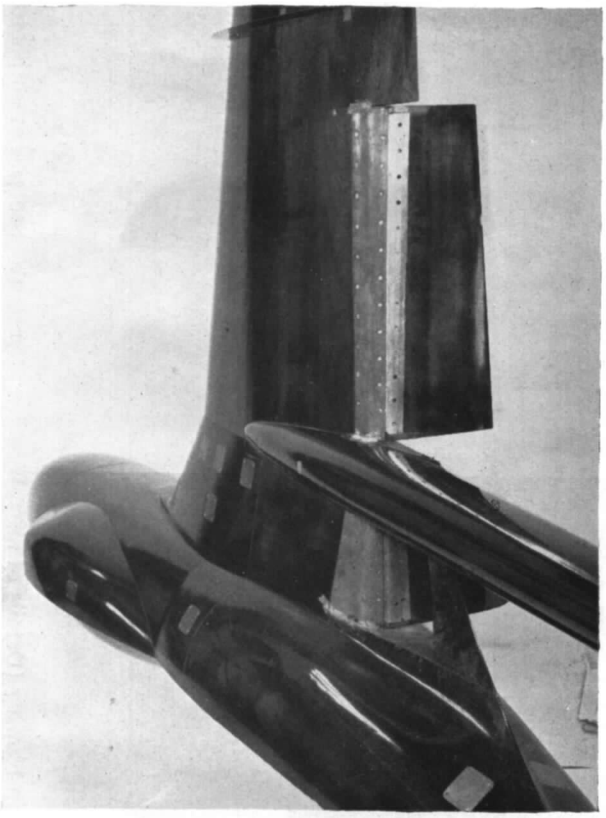

FIG. 3. Rear view of model showing flap and nozzle details.

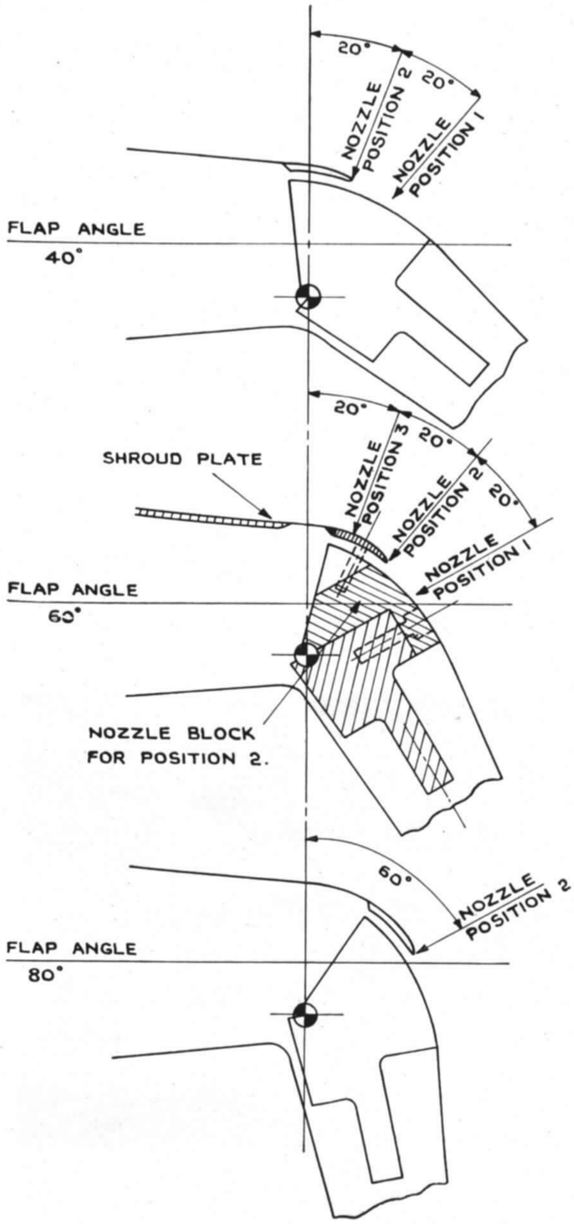

FIG. 4. Sections at inboard end of outboard flap on model (Drawn for position 2 at each flap angle).

(75640) C

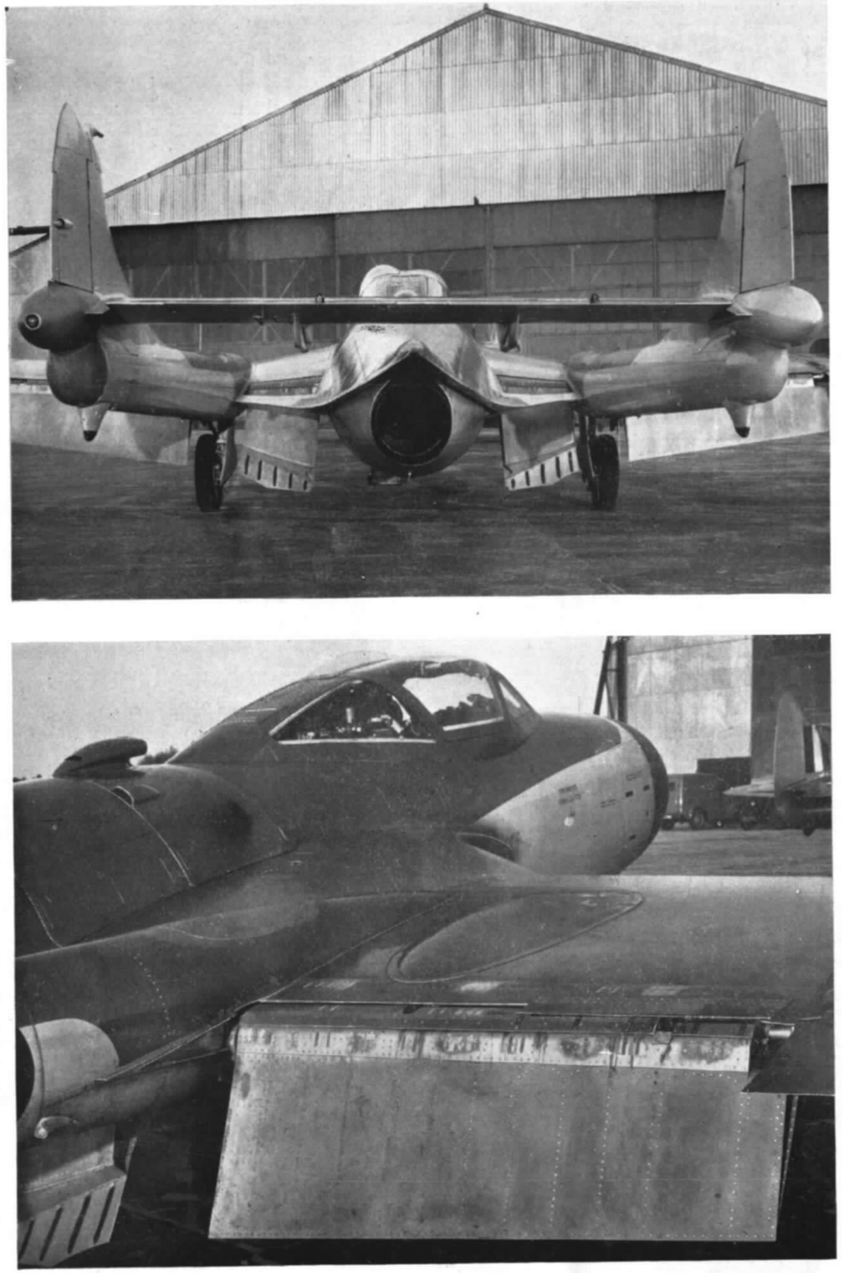

FIG. 5. De Havilland *Sea Venom* with flap blowing (Details of aircraft installation).

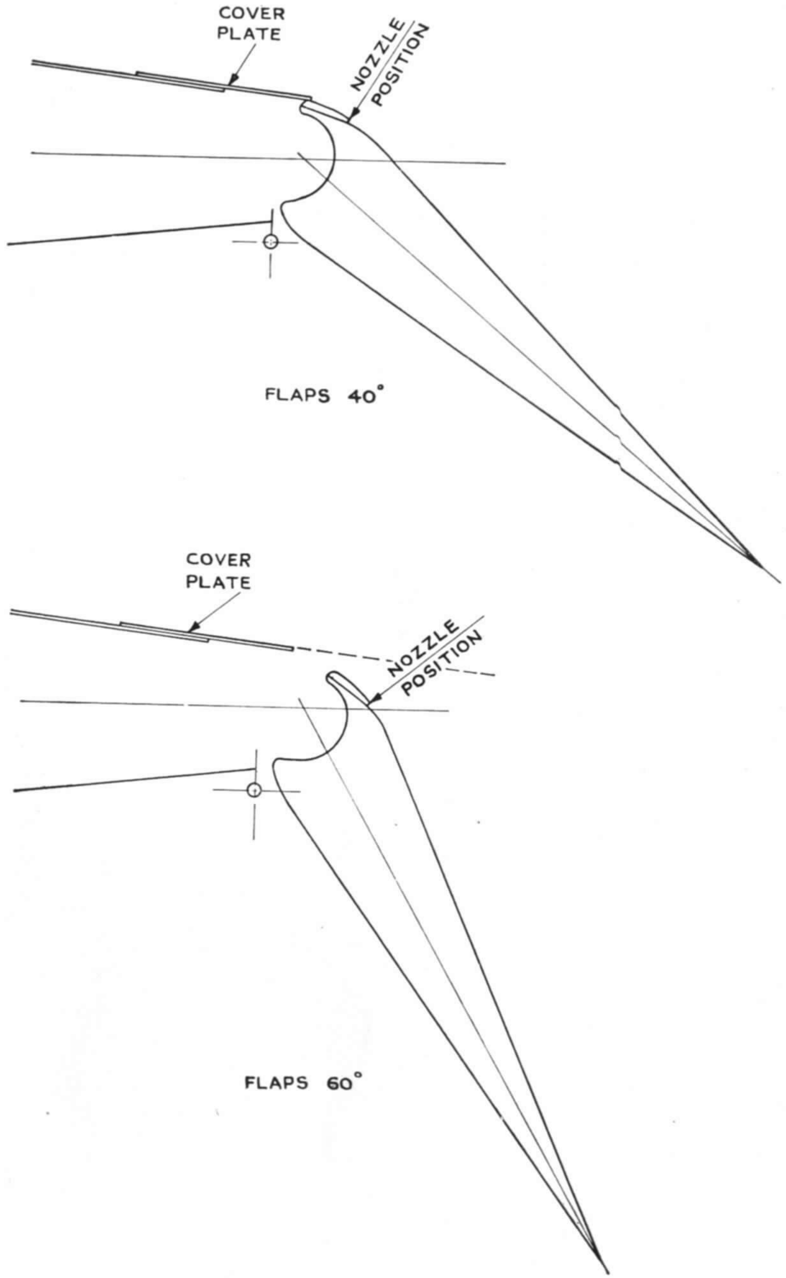

FIG. 6. Sections at outboard end of outboard flap on aircraft.

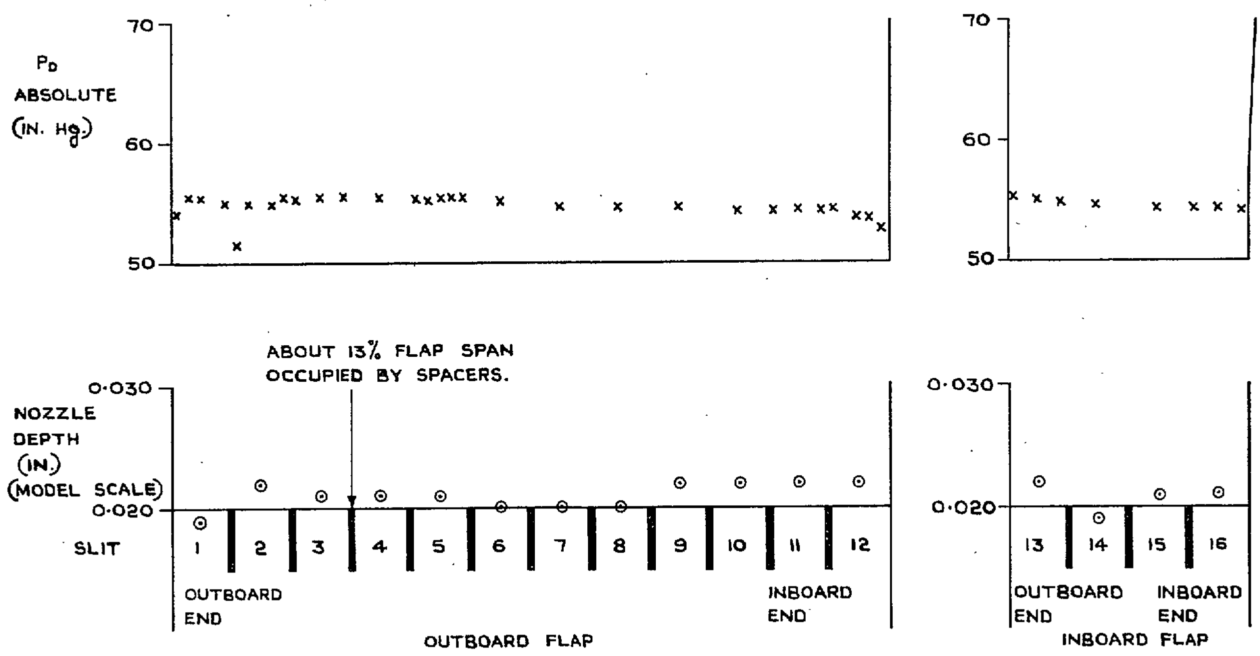

FIG. 7. Typical spanwise distributions of total head and nozzle depth on tunnel model.

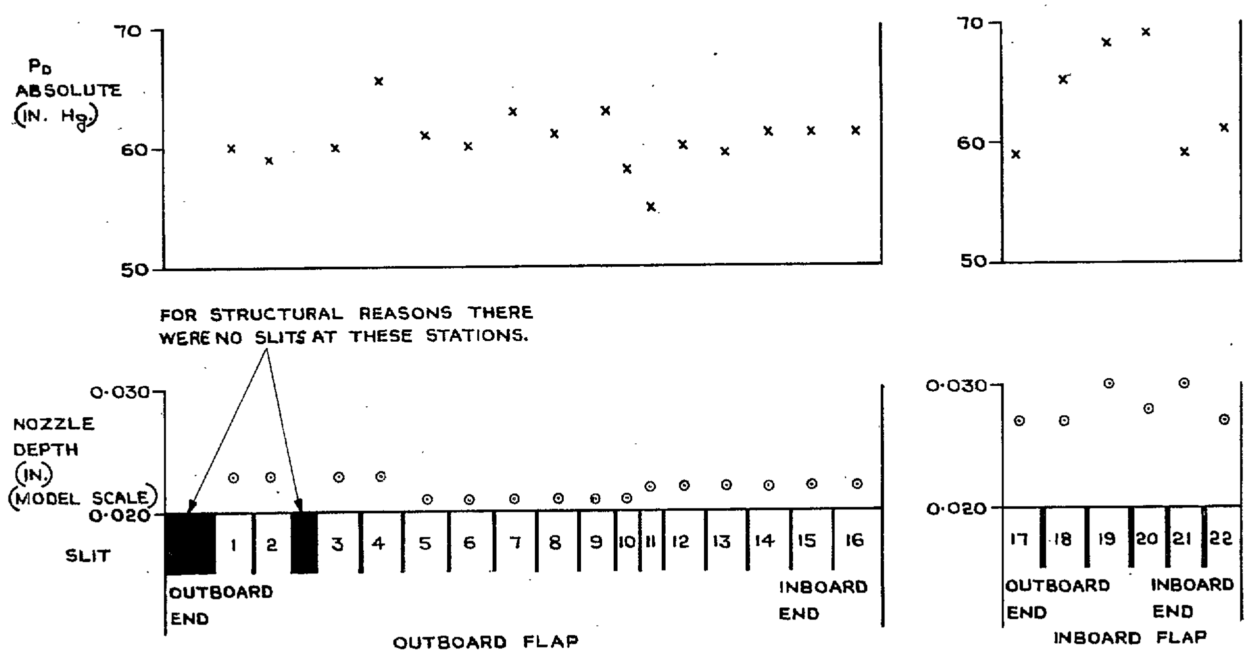

FIG. 8. Typical spanwise distributions of total head and nozzle depth on aircraft.

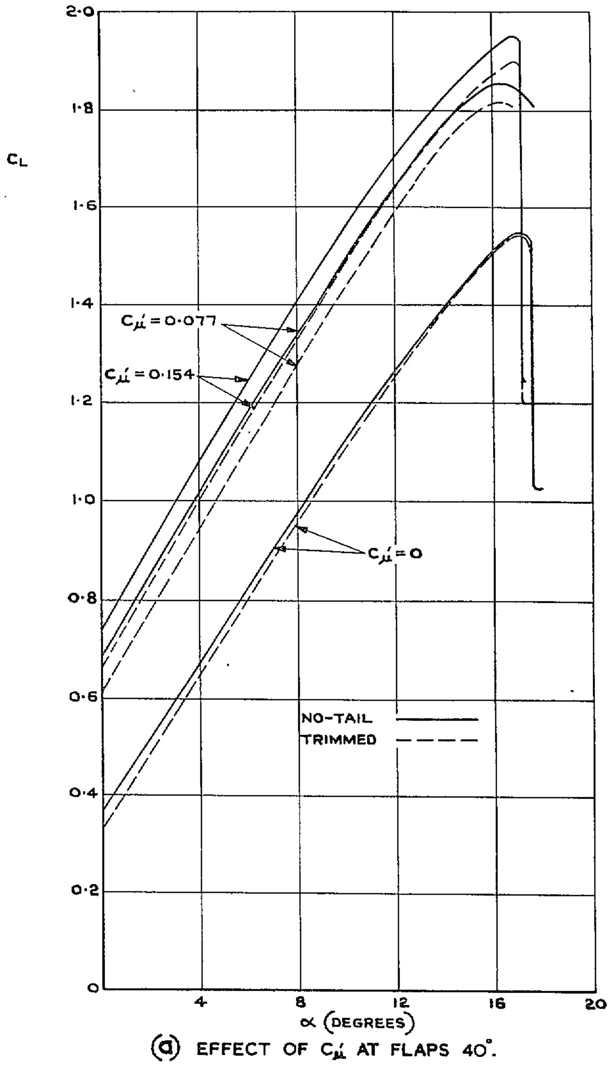

(a) EFFECT OF C_μ' AT FLAPS 40°.

FIG. 9a. C_L vs. α.

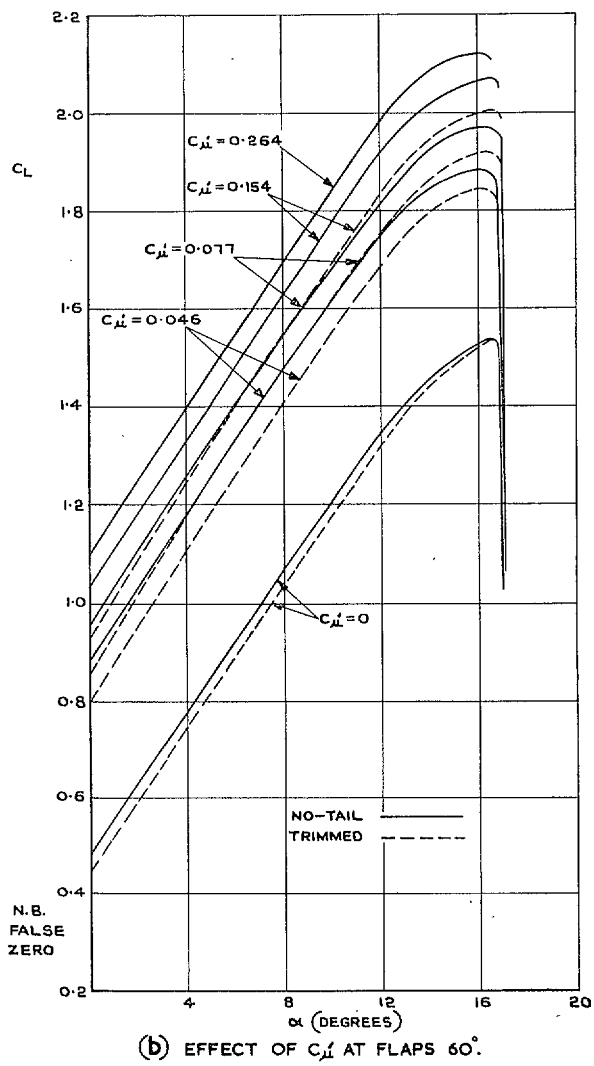

(b) EFFECT OF C_μ' AT FLAPS 60°.

FIG. 9b. C_L vs. α.

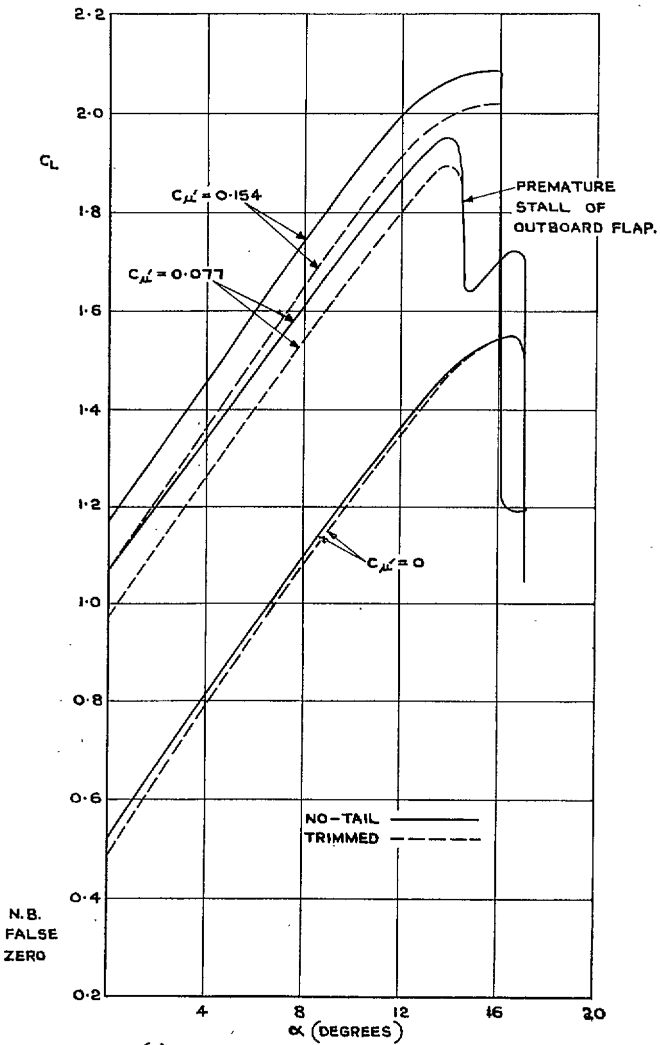

(c) EFFECT OF C_μ' AT FLAPS 80°.

FIG. 9c. C_L vs. α.

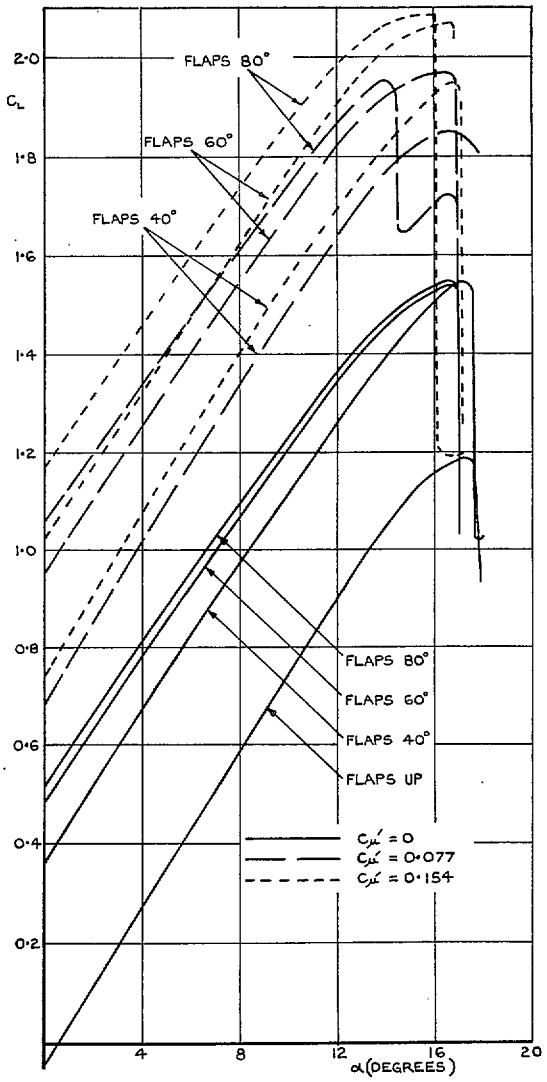

(d) COMBINED EFFECT OF FLAP ANGLE AND C_μ' (NO-TAIL).

FIG. 9d. C_L vs. α.

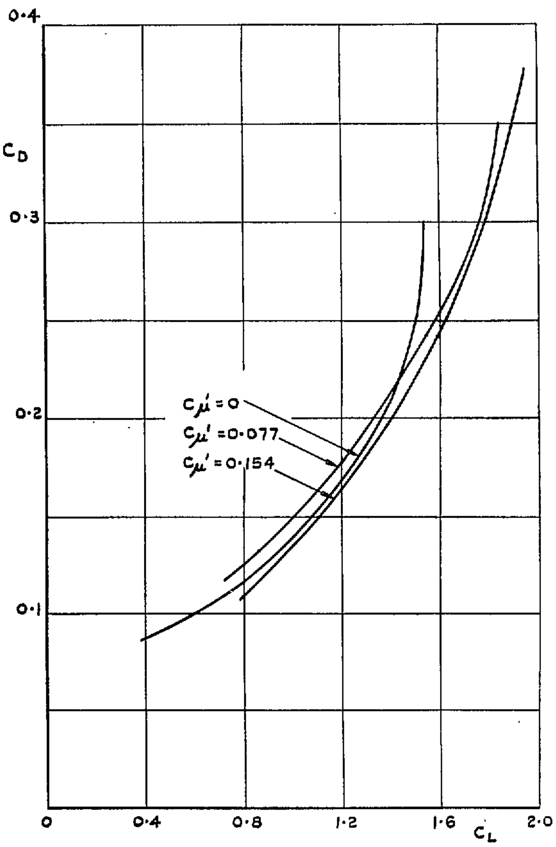

(a) EFFECT OF C_μ' AT FLAPS 40°
(NO-TAIL).

FIG. 10a. C_D vs. C_L.

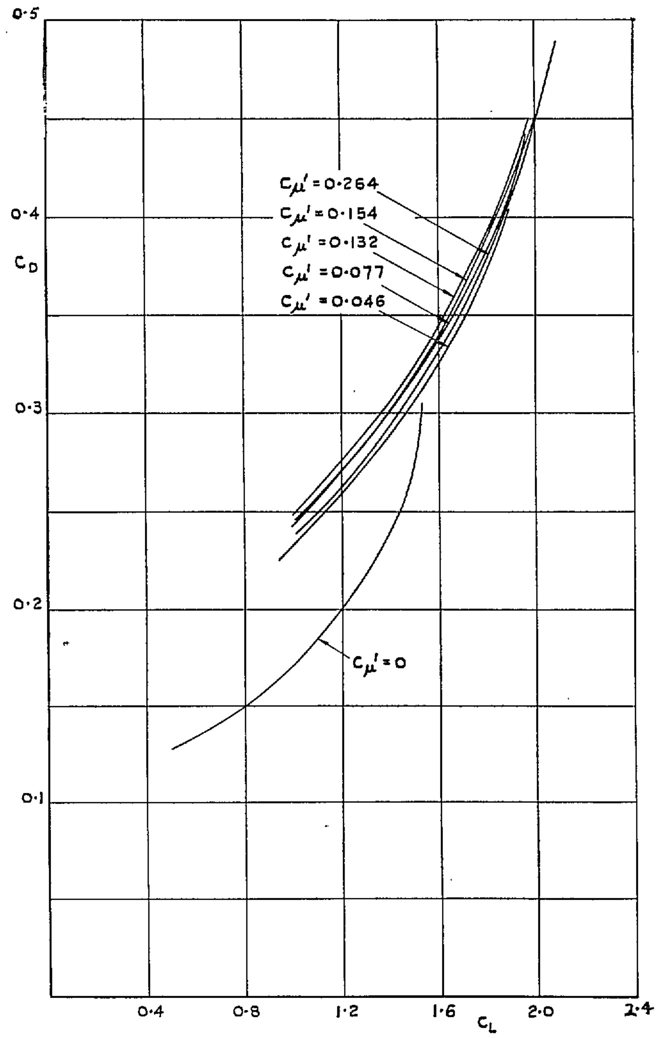

(b) EFFECT OF C_μ' AT FLAPS 60°
(NO-TAIL).

FIG. 10b. C_D vs. C_L.

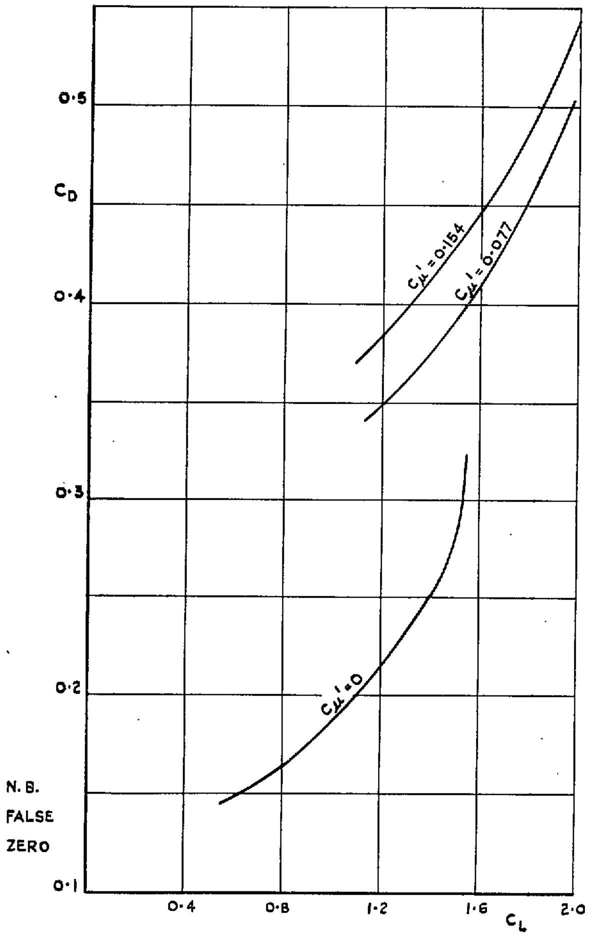

(c) EFFECT OF C_μ' AT FLAPS 80° (NO-TAIL).

FIG. 10c. C_D vs. C_L.

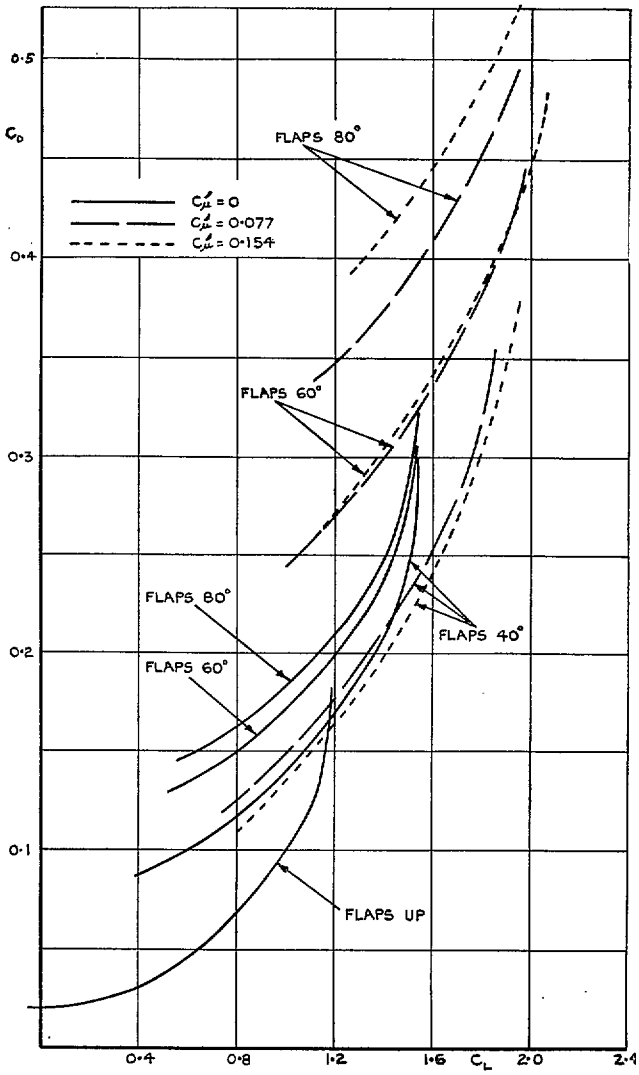

(d) COMBINED EFFECT OF FLAP ANGLE AND C_μ' (NO-TAIL).

FIG. 10d. C_D vs. C_L.

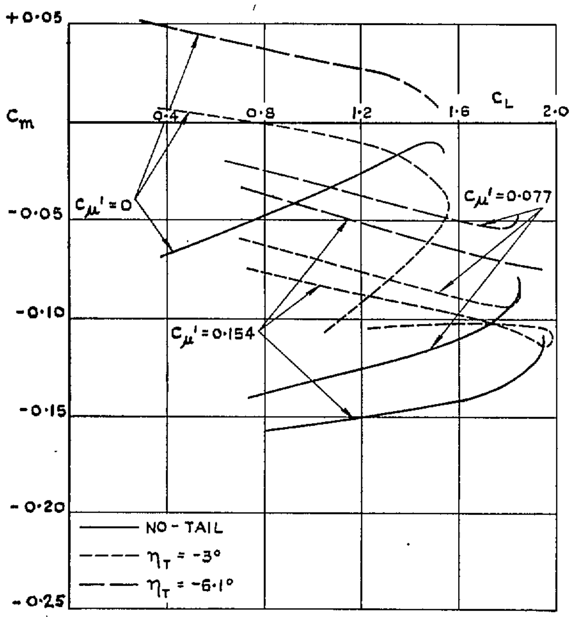

(a) EFFECT OF $C_\mu{}'$ AT FLAPS 40°.

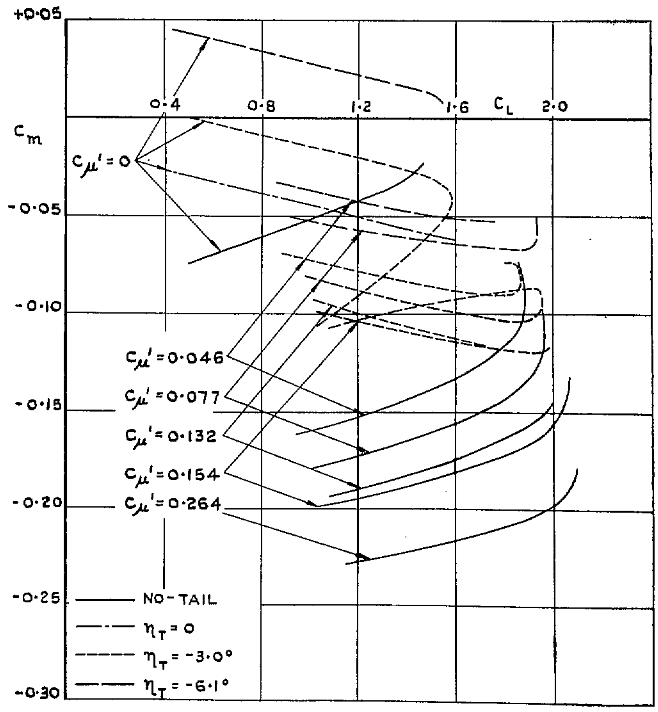

(b) EFFECT OF $C_\mu{}'$ AT FLAPS 60°.

FIG. 11a. C_m vs. C_L.

FIG. 11b. C_m vs. C_L.

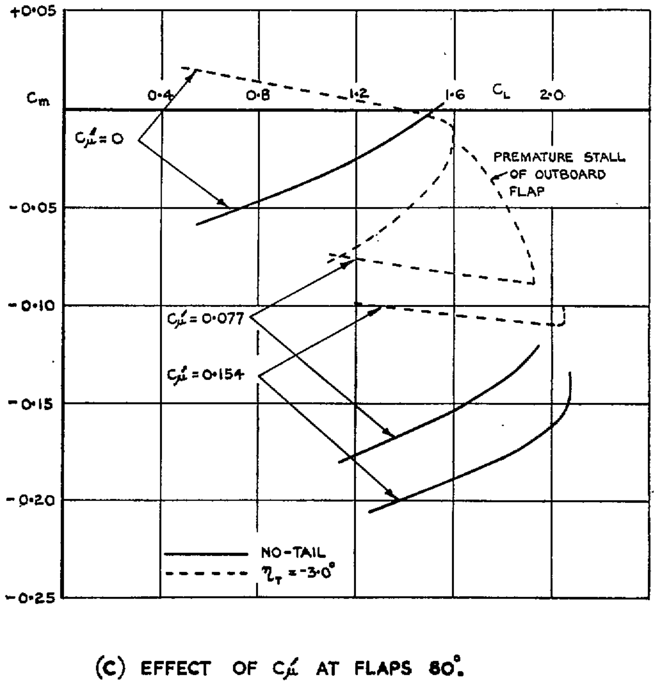

FIG. 11c. C_m vs. C_L.

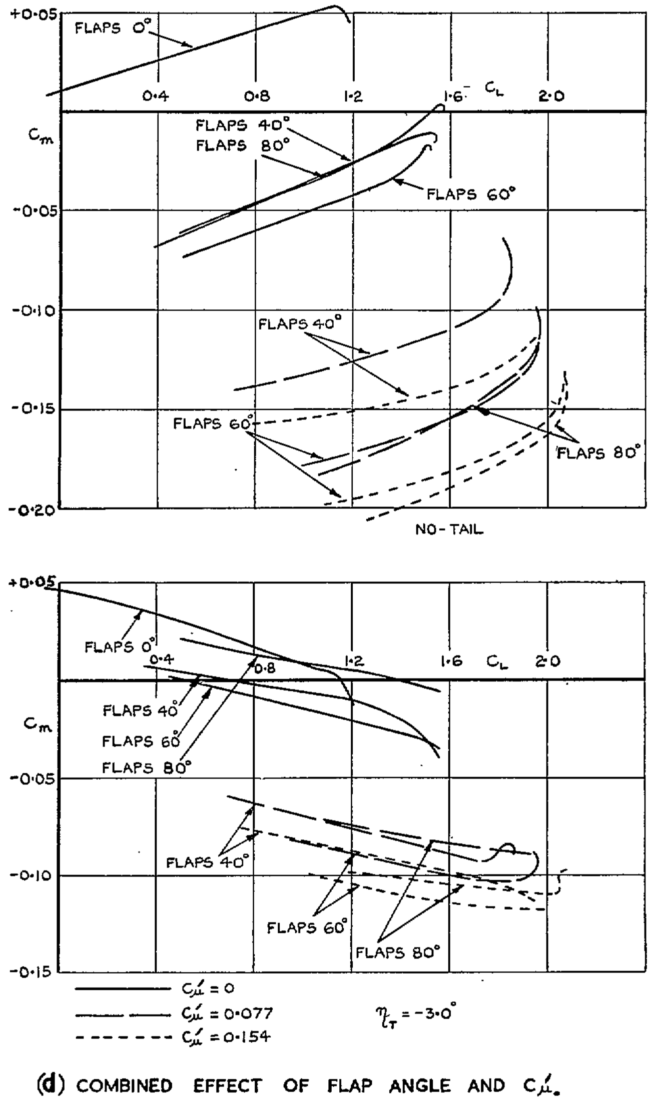

FIG. 11d. C_m vs. C_L.

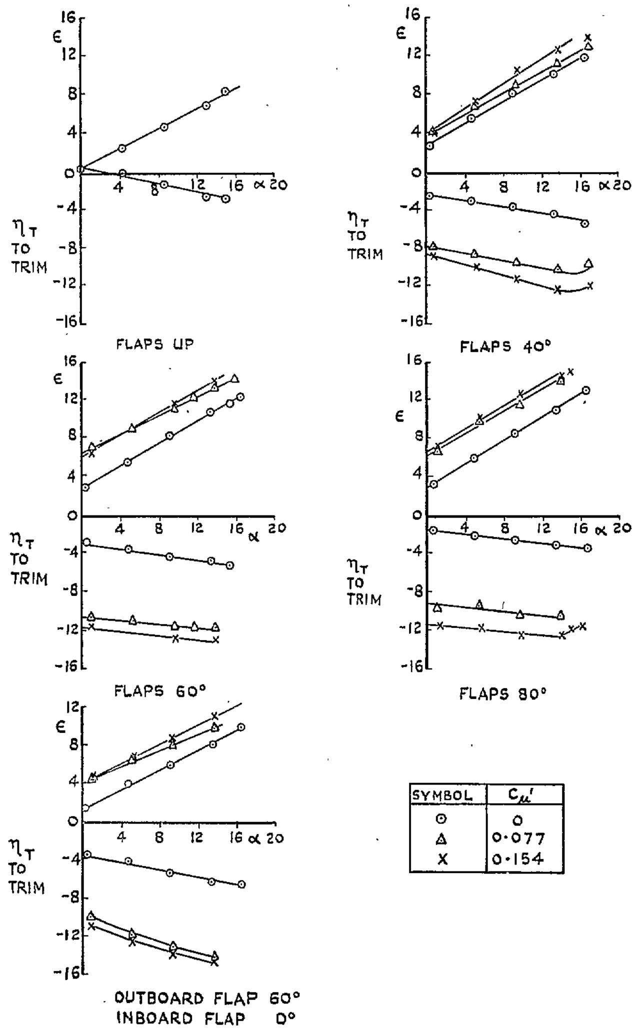

FIG. 12. Downwash at tail and η_T to trim versus α.

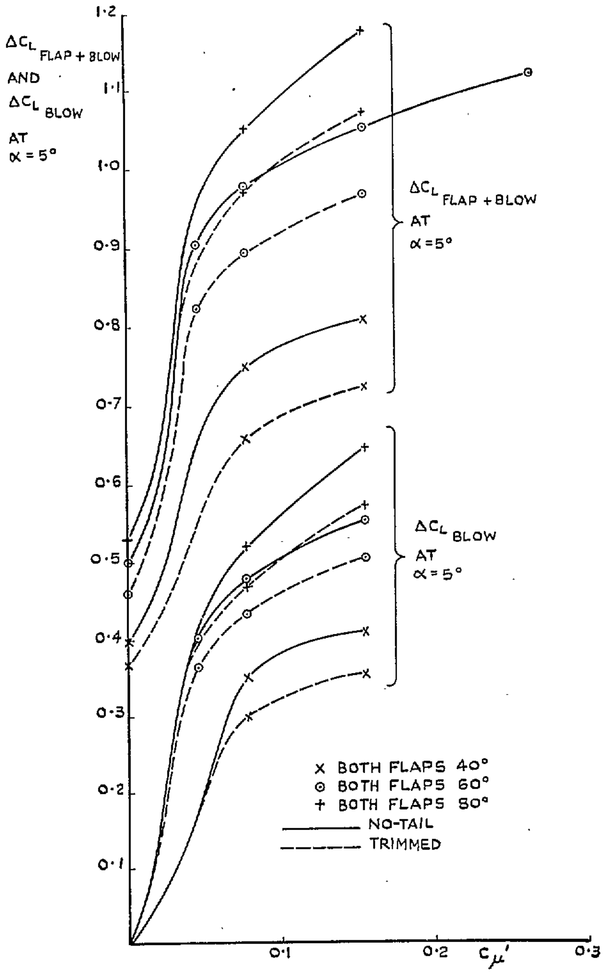

Fig. 13. Variation with C_{μ}' of lift increments at $\alpha = 5$ deg produced by blowing over both flaps at flap angles of 40, 60, and 80 deg (Standard condition).

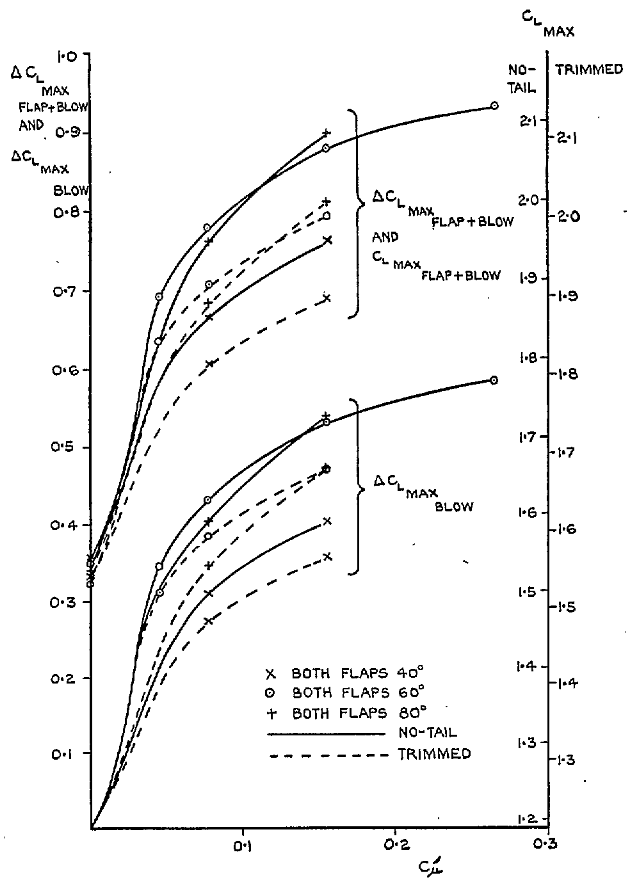

Fig. 14. Variation with C_{μ}' of maximum-lift increments and $C_{L\max}$ produced by blowing over both flaps at flap angles of 40, 60, and 80 deg (Standard condition).

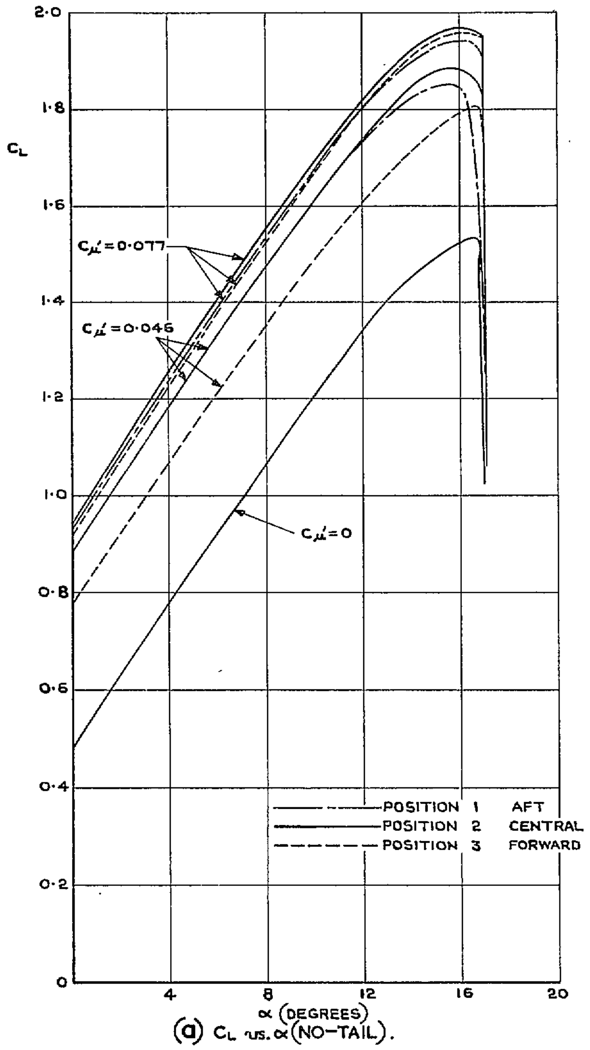

FIG. 15a. Effect of nozzle position at flaps 60 deg.

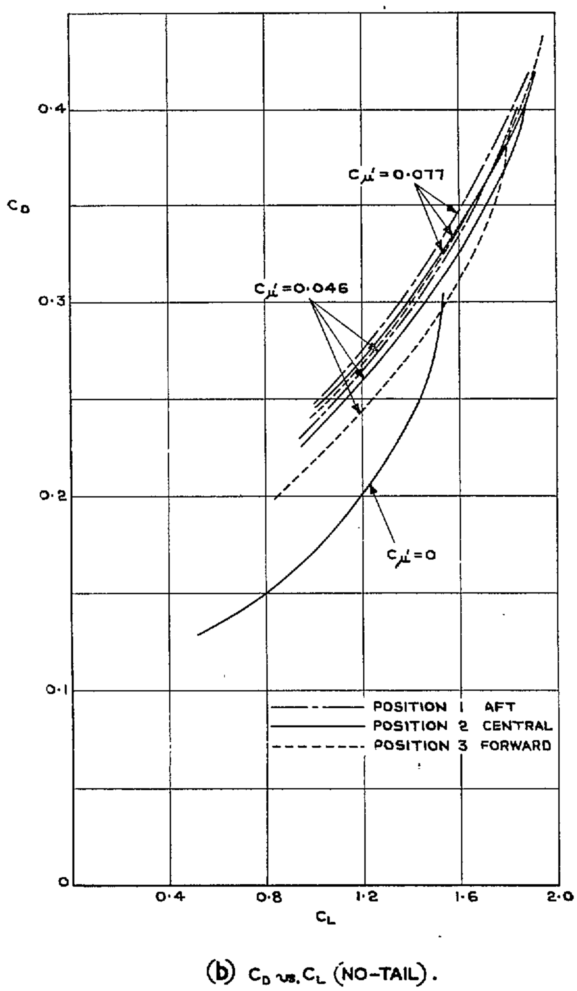

FIG. 15b. Effect of nozzle position at flaps 60 deg.

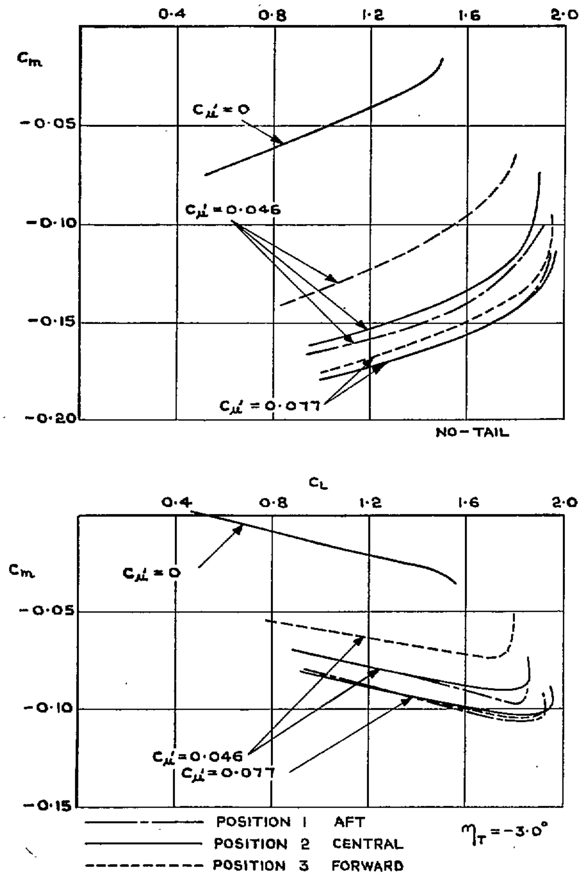

(c) C_m vs. C_L.

FIG. 15c. Effect of nozzle position at flaps 60 deg.

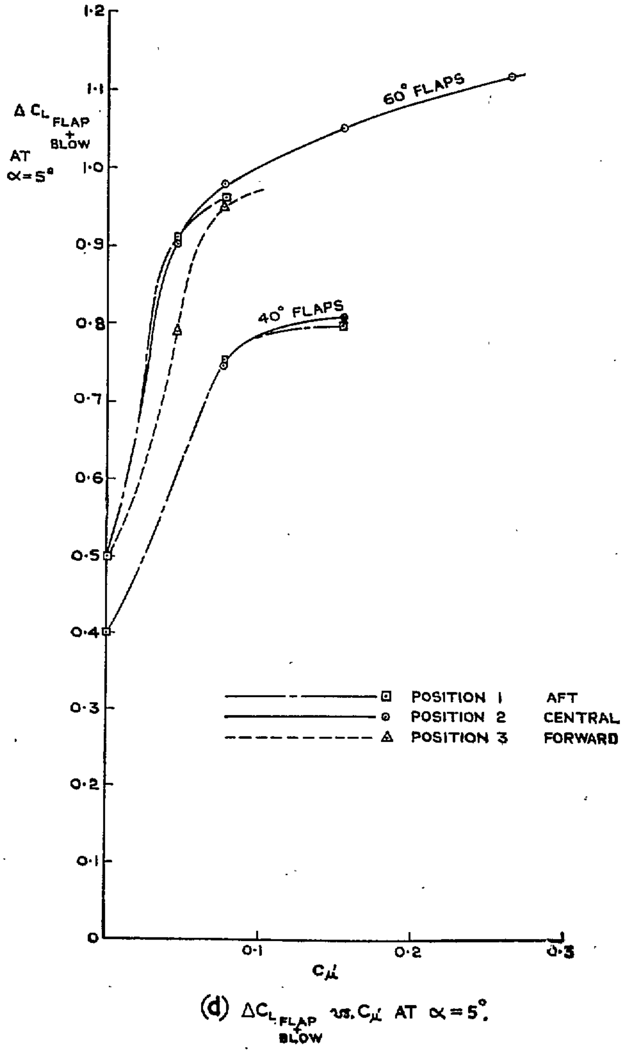

(d) $\Delta C_{L_{\substack{FLAP\\+\\BLOW}}}$ vs. C_{μ}' AT $\alpha = 5°$.

FIG. 15d. Effect of nozzle position at flaps 40 and 60 deg.

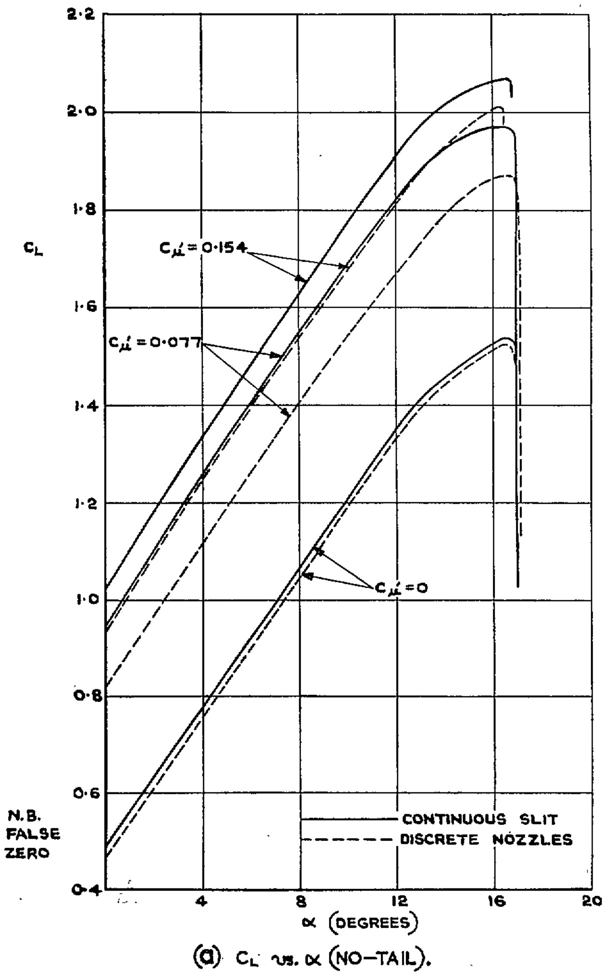

FIG. 16a. Comparison between blowing through discrete nozzles and blowing through a continuous slit (Flaps 60 deg).

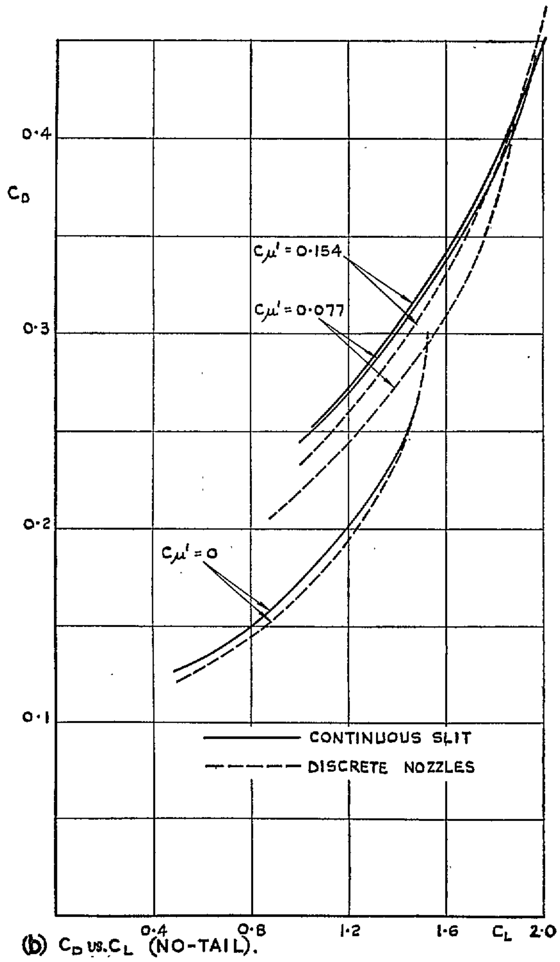

FIG. 16b. Comparison between blowing through discrete nozzles and blowing through a continuous slit (Flaps 60 deg).

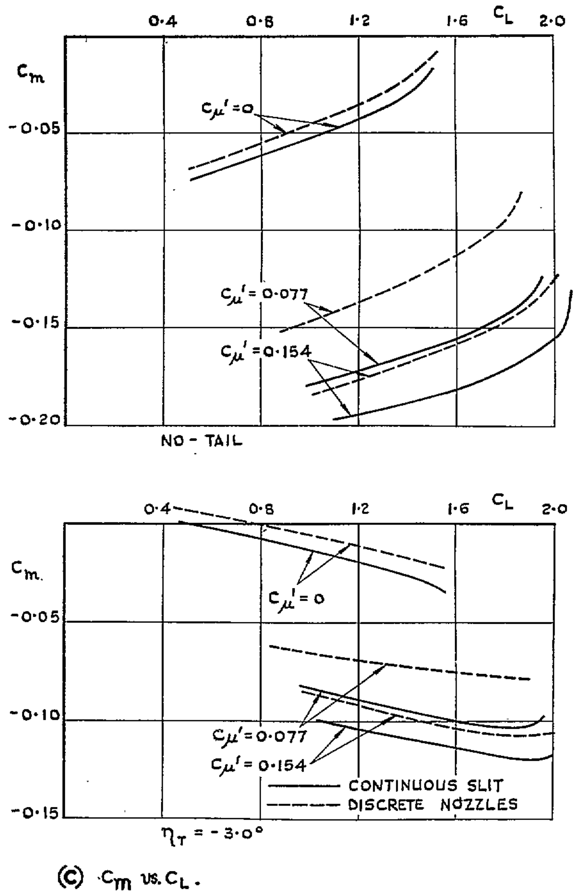

FIG. 16c. Comparison between blowing through discrete nozzles and blowing through a continuous slit (Flaps 60 deg).

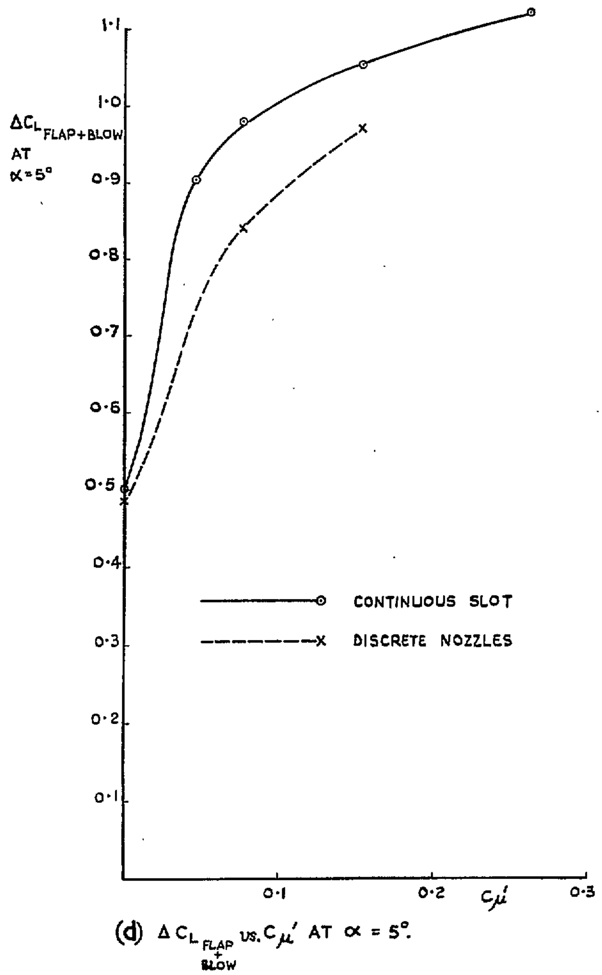

FIG. 16d. Comparison between blowing through discrete nozzles and blowing through a continuous slit (Flaps 60 deg).

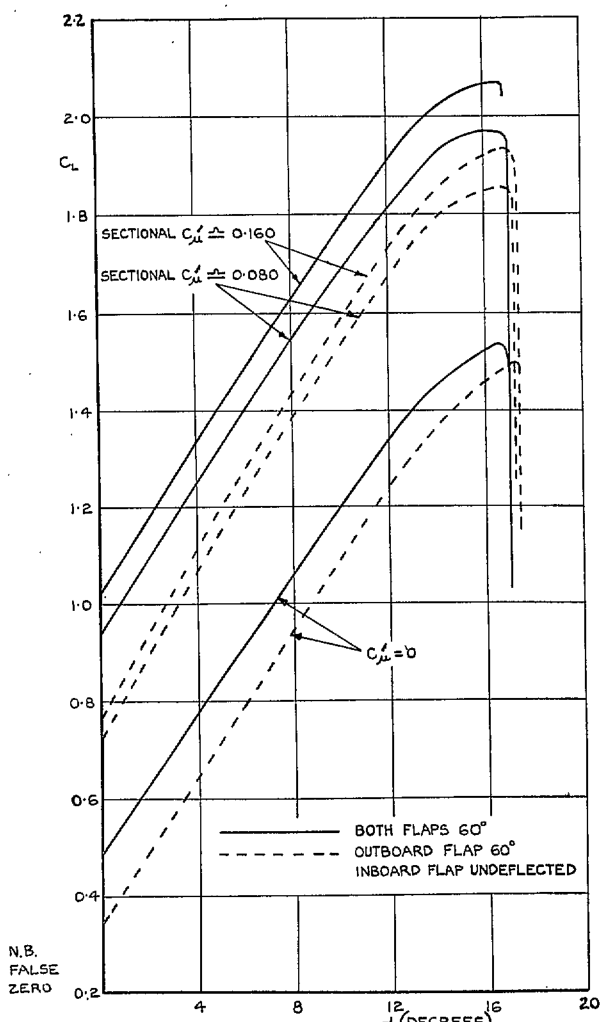

(a) C_L vs. α (NO-TAIL).

FIG. 17a. Comparison between blowing over the outboard flap only and blowing over both flaps.

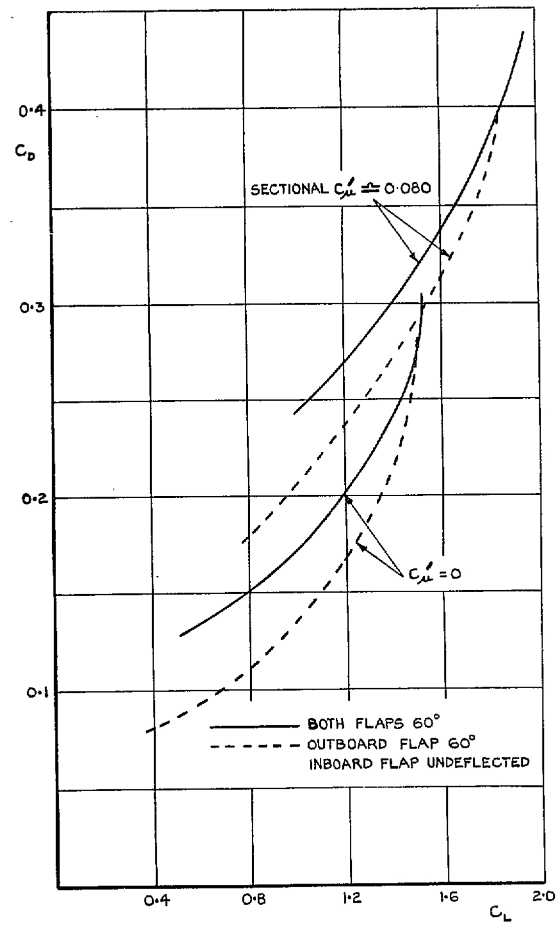

(b) C_D vs. C_L (NO-TAIL).

FIG. 17b. Comparison between blowing over the outboard flap only and blowing over both flaps.

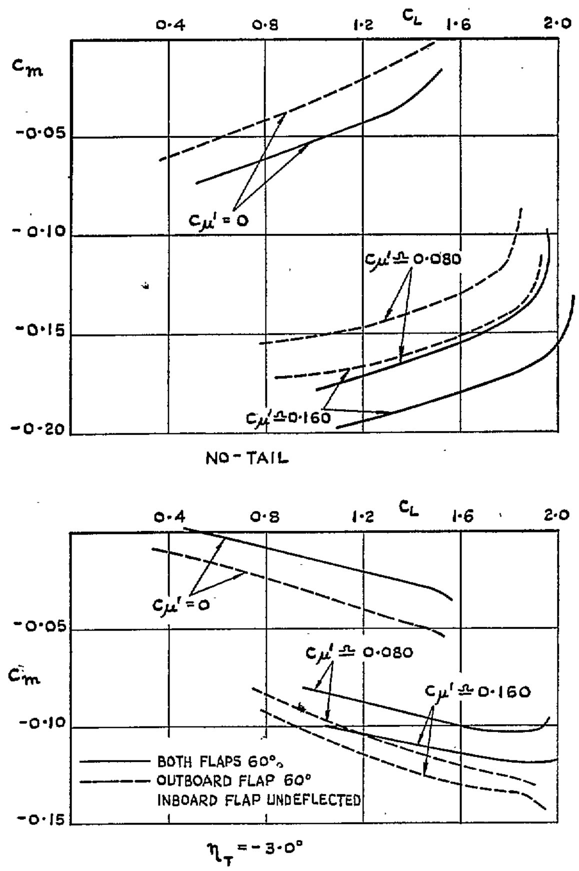

(c) C_m vs. C_L.

Fig. 17c. Comparison between blowing over the outboard flap only and blowing over both flaps.

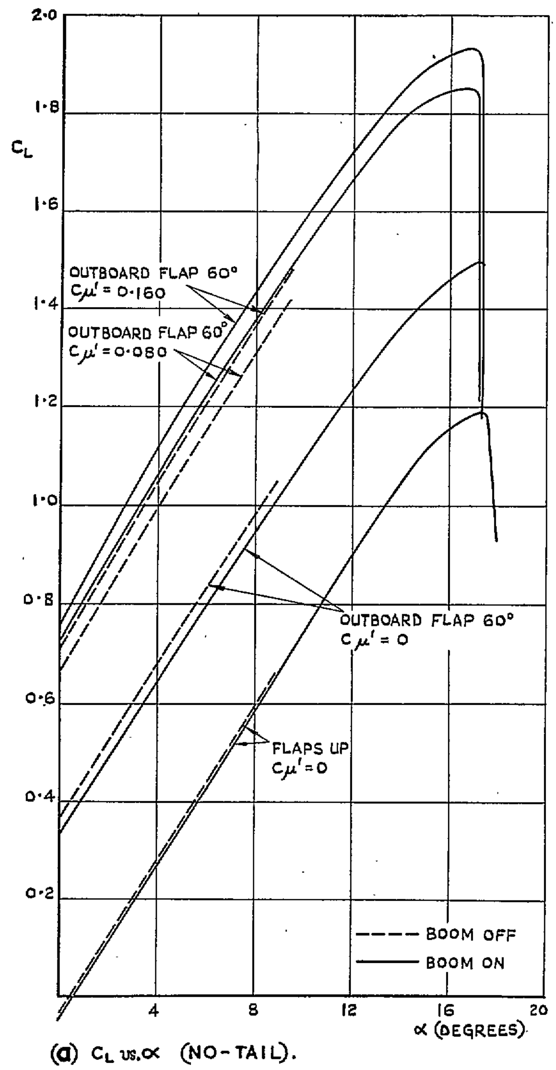

(a) C_L vs. α (NO-TAIL).

FIG. 18a. Effect of removing boom with blowing over the outboard flap only.

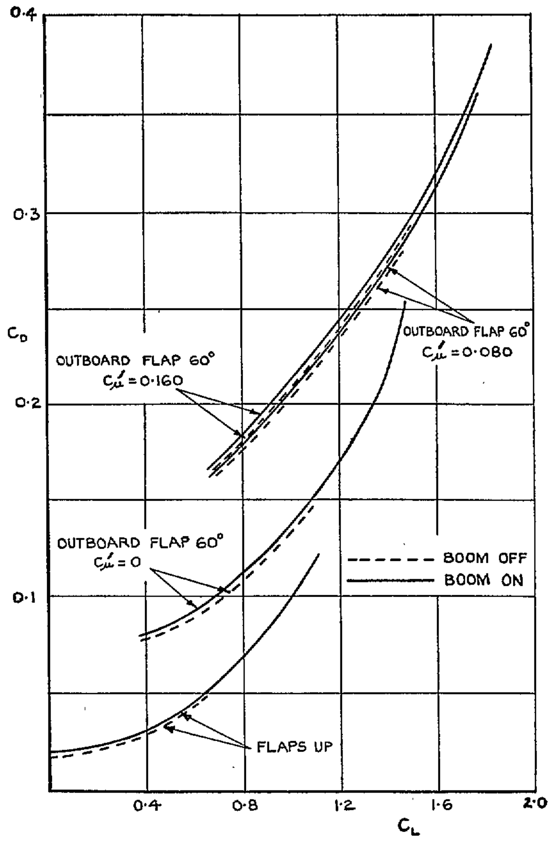

(b) C_D vs. C_L (NO-TAIL).

FIG. 18b. Effect of removing boom with blowing over the outboard flap only.

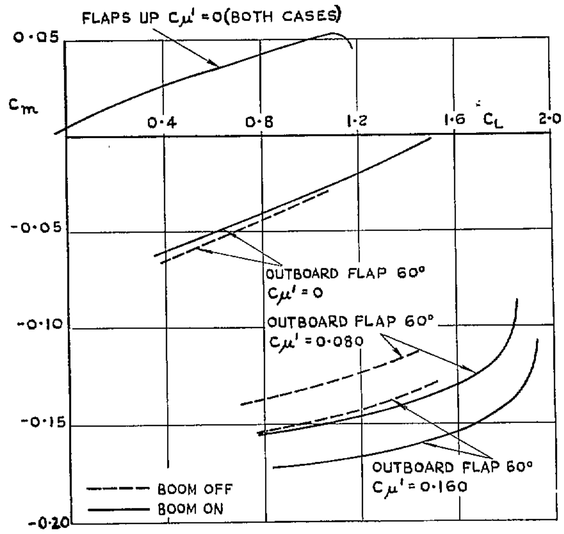

(c) C_m vs. C_L (NO-TAIL).

FIG. 18c. Effect of removing boom with blowing over the outboard flap only.

	FLAP ANGLE INBOARD	FLAP ANGLE OUTBOARD	FLAPS BLOWN	HOOK BAR	BOOM
x	60°	60°	BOTH	OFF	ON
⊙	60°	60°	BOTH	ON	ON
⊡	0°	60°	OUTBOARD	ON	ON
◇	0°	60°	OUTBOARD	ON	OFF

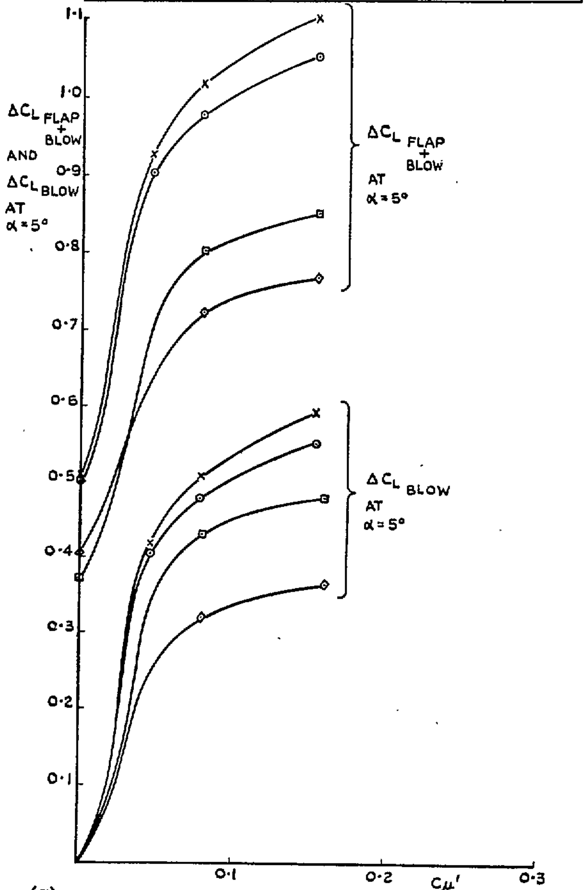

(a) ON A SECTIONAL MOMENTUM COEFFICIENT BASIS.

FIG. 19a. Comparison of lift increments at $\alpha = 5$ deg produced by blowing over outboard flap and by blowing over both flaps (Flap angle of 60 deg).

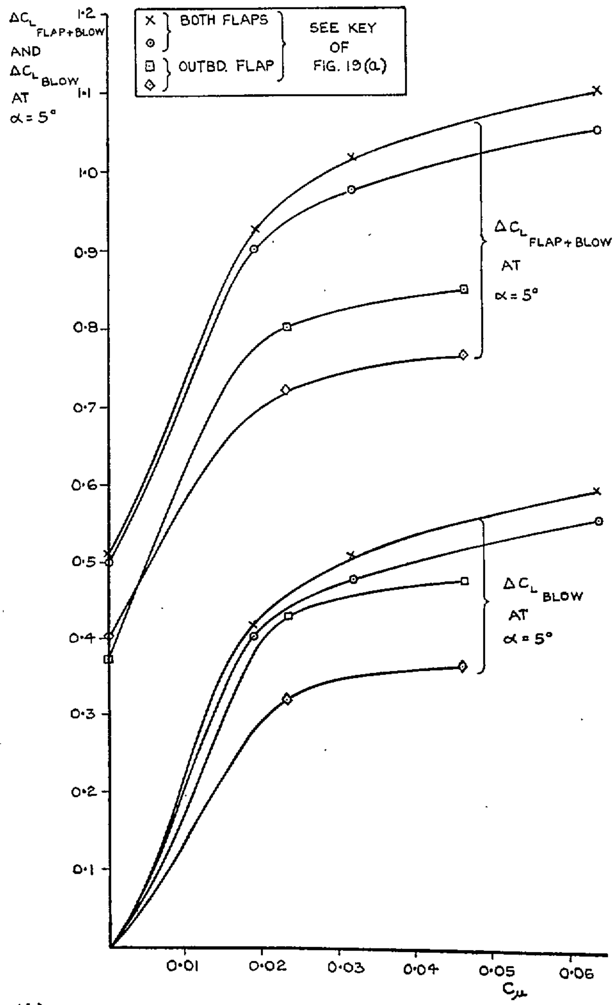

(b) MOMENTUM COEFFICIENT BASED ON GROSS WING AREA.

FIG. 19b. Comparison of lift increments at $\alpha = 5$ deg produced by blowing over outboard flap and by blowing over both flaps (Flap angle of 60 deg).

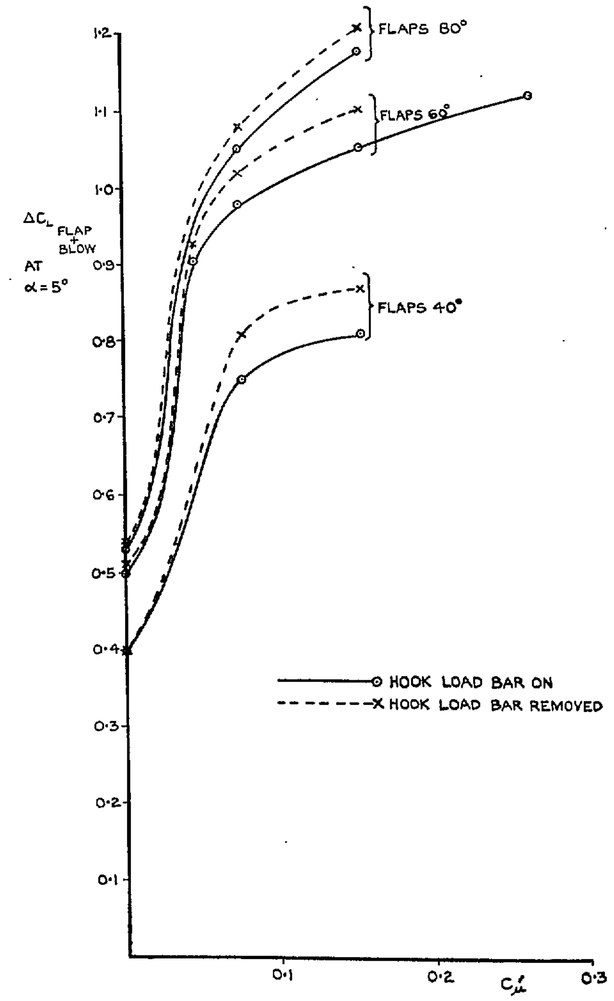

FIG. 20. The effect of the hook-load side bar on $\Delta C_{L\,(\mathrm{Flap}\,+\,\mathrm{Blow})}$ at $\alpha = 5$ deg.

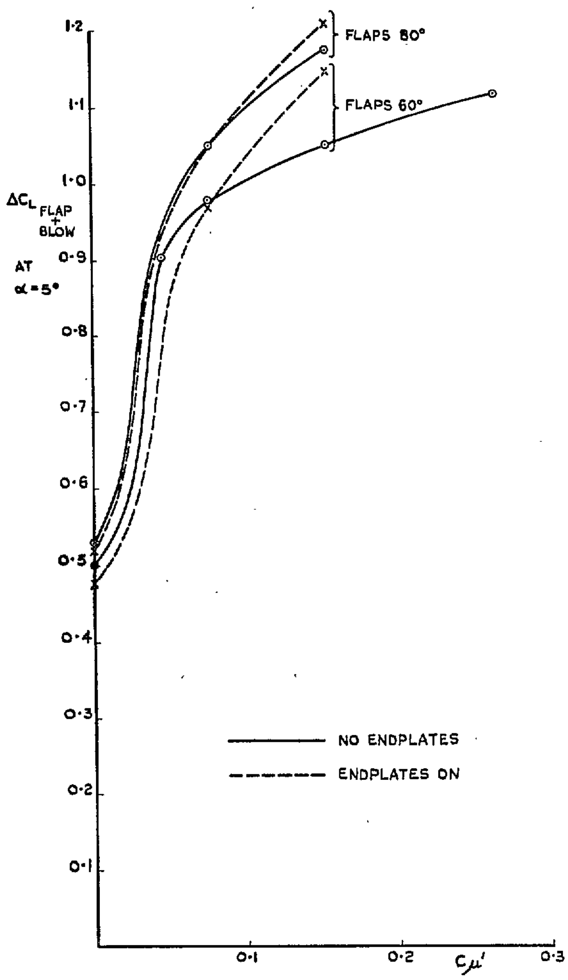

FIG. 21. The effect of end plates on $\Delta C_{L\,(\mathrm{Flap}\,+\,\mathrm{Blow})}$ at $\alpha = 5$ deg.

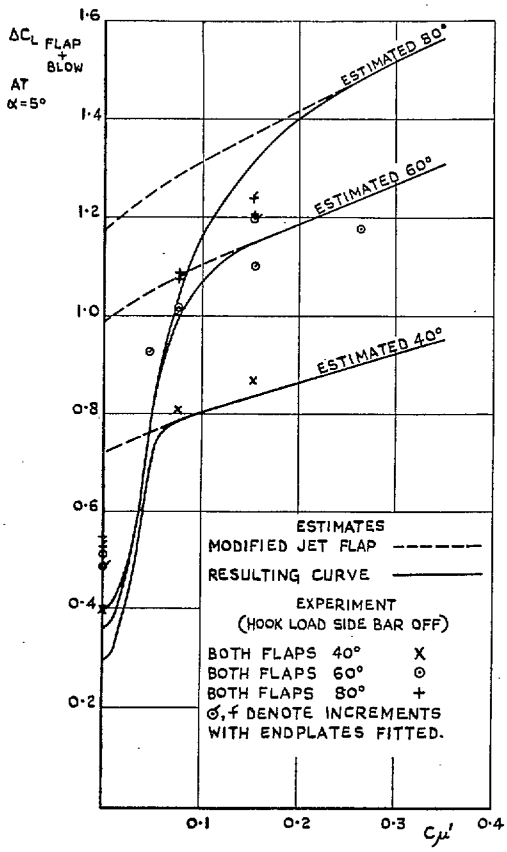

(a) BLOWING OVER BOTH FLAPS (BOOM ON).

FIG. 22a. Comparison between estimated and measured no-tail values of $\Delta C_{L\,(\mathrm{Flap}\,+\,\mathrm{Blow})}$ at $\alpha = 5$ deg.

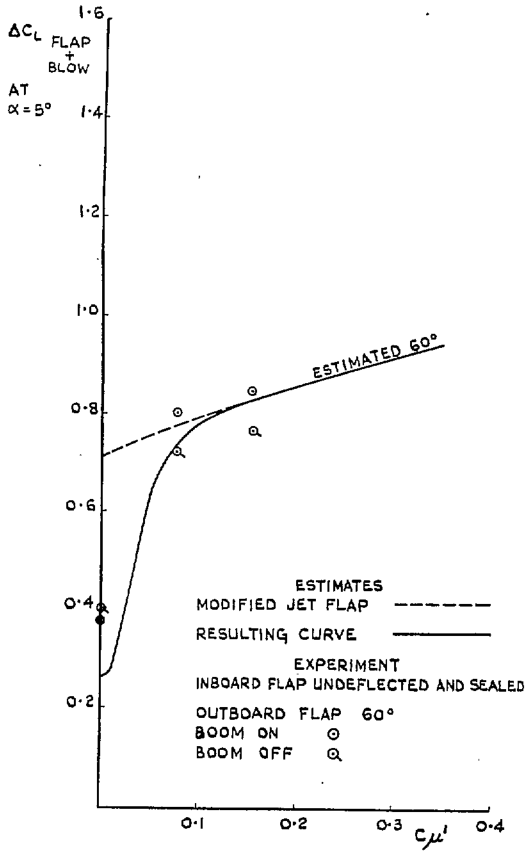

(b) BLOWING OVER OUTBOARD FLAP ONLY.

FIG. 22b. Comparison between estimated and measured no-tail values of $\Delta C_{L\,(\mathrm{Flap}\,+\,\mathrm{Blow})}$ at $\alpha = 5$ deg.

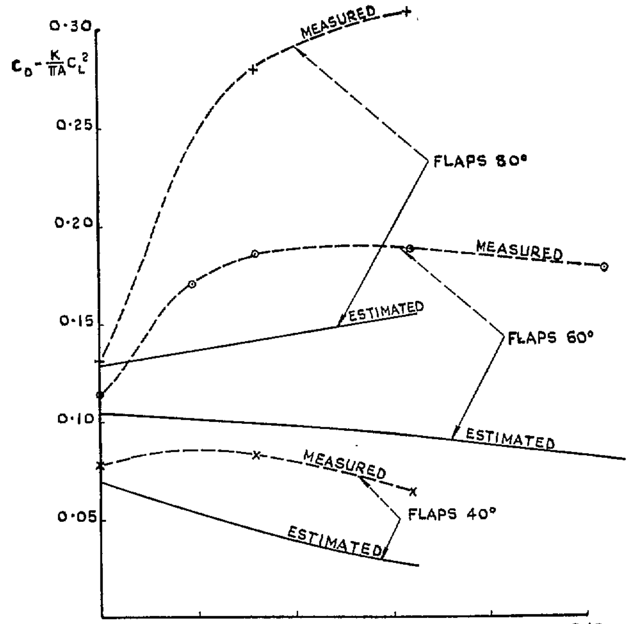

(a) BLOWING OVER BOTH FLAPS.

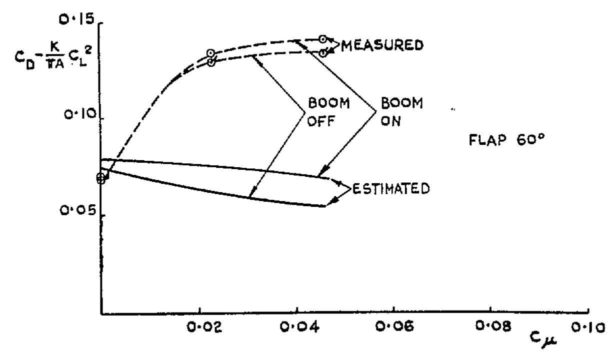

(b) BLOWING OVER OUTBOARD FLAP ONLY.

FIGS. 23a and 23b. Comparison between estimated and measured no-tail values of $[C_D - K/\pi A \,.\, C_L^2]$ at low incidences.

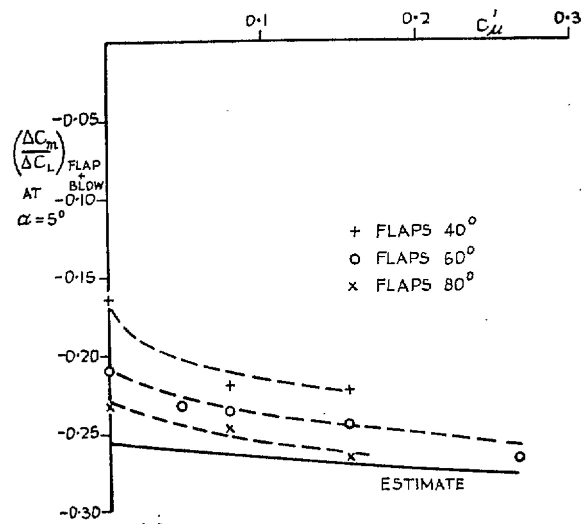

(a) BLOWING OVER BOTH FLAPS.

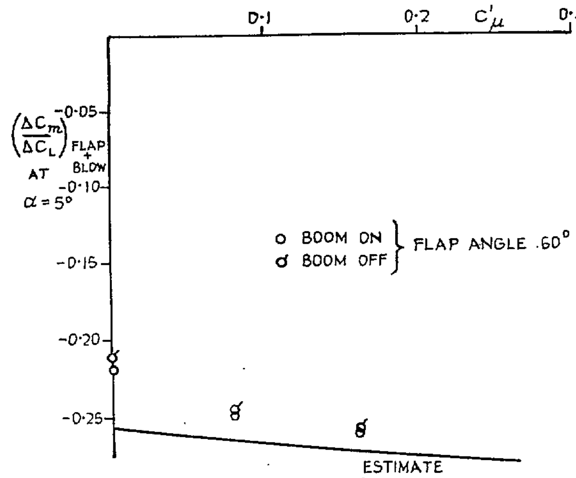

(b) BLOWING OVER OUTBOARD FLAP ONLY.

FIGS. 24a and 24b. Comparison between estimated and measured no-tail values of $(\Delta C_m/\Delta C_L)_{(\text{Flap + Blow})}$.

(75640) Wt. 53/2293 K.7 11/59 Hw.

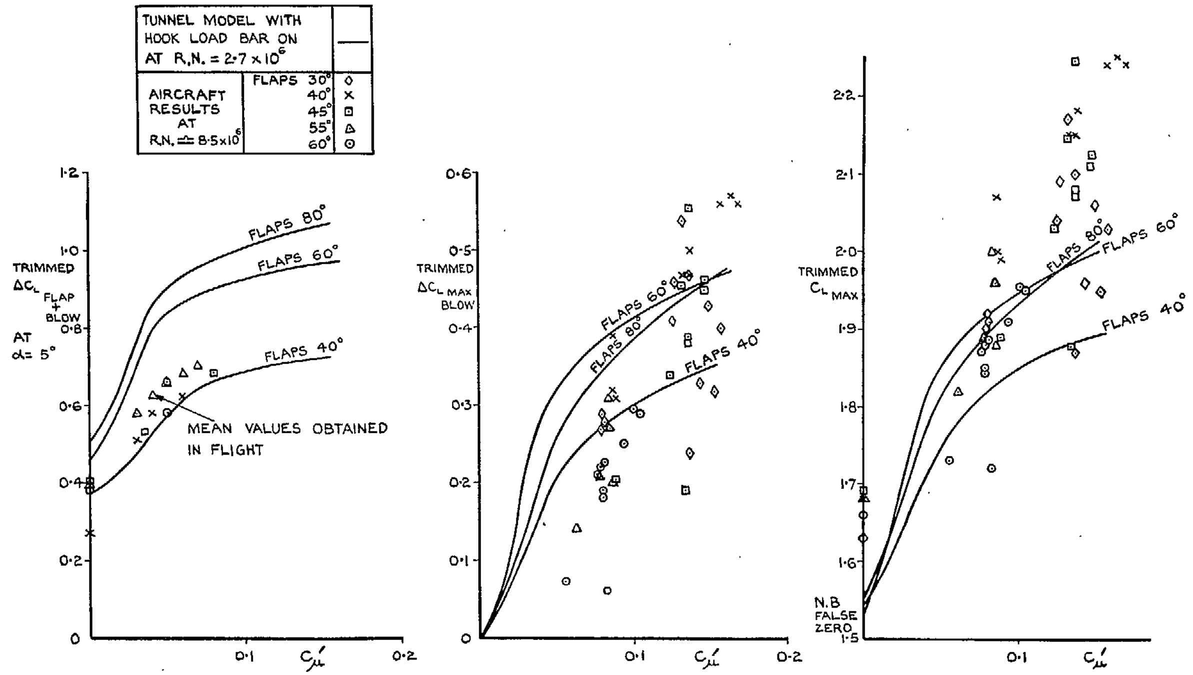

FIG. 25. Flight/tunnel comparison of lift increments.

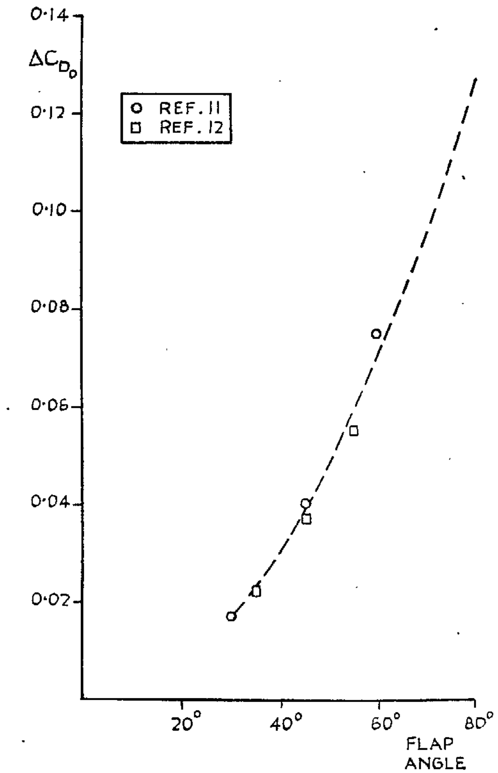

FIG. 26. Flap sectional profile-drag coefficients for 27 per cent chord plain flaps with blowing (two-dimensional tests).

PRINTED IN GREAT BRITAIN

Publications of the Aeronautical Research Council

ANNUAL TECHNICAL REPORTS OF THE AERONAUTICAL RESEARCH COUNCIL (BOUND VOLUMES)

1939 Vol. I. Aerodynamics General, Performance, Airscrews, Engines. 50*s.* (52*s.*).
Vol. II. Stability and Control, Flutter and Vibration, Instruments, Structures, Seaplanes, etc. 63*s.* (65*s.*)

1940 Aero and Hydrodynamics, Aerofoils, Airscrews, Engines, Flutter, Icing, Stability and Control, Structures, and a miscellaneous section. 50*s.* (52*s.*)

1941 Aero and Hydrodynamics, Aerofoils, Airscrews, Engines, Flutter, Stability and Control, Structures. 63*s.* (65*s.*)

1942 Vol. I. Aero and Hydrodynamics, Aerofoils, Airscrews, Engines. 75*s.* (77*s.*)
Vol. II. Noise, Parachutes, Stability and Control, Structures, Vibration, Wind Tunnels. 47*s.* 6*d.* (49*s.* 6*d.*)

1943 Vol. I. Aerodynamics, Aerofoils, Airscrews. 80*s.* (82*s.*)
Vol. II. Engines, Flutter, Materials, Parachutes, Performance, Stability and Control, Structures. 90*s.* (92*s.* 9*d.*)

1944 Vol. I. Aero and Hydrodynamics, Aerofoils, Aircraft, Airscrews, Controls. 84*s.* (86*s.* 6*d.*)
Vol. II. Flutter and Vibration, Materials, Miscellaneous, Navigation, Parachutes, Performance, Plates and Panels, Stability, Structures, Test Equipment, Wind Tunnels. 84*s.* (86*s.* 6*d.*)

1945 Vol. I. Aero and Hydrodynamics, Aerofoils. 130*s.* (132*s.* 9*d.*)
Vol. II. Aircraft, Airscrews, Controls. 130*s.* (132*s.* 9*d.*)
Vol. III. Flutter and Vibration, Instruments, Miscellaneous, Parachutes, Plates and Panels, Propulsion. 130*s.* (132*s.* 6*d.*)
Vol. IV. Stability, Structures, Wind Tunnels, Wind Tunnel Technique. 130*s.* (132*s.* 6*d.*)

Annual Reports of the Aeronautical Research Council—

1937 2*s.* (2*s.* 2*d.*) 1938 1*s.* 6*d.* (1*s.* 8*d.*) 1939–48 3*s.* (3*s.* 5*d.*)

Index to all Reports and Memoranda published in the Annual Technical Reports, and separately—

April, 1950 - - - - - R. & M. 2600 2*s.* 6*d.* (2*s.* 10*d.*)

Author Index to all Reports and Memoranda of the Aeronautical Research Council—

1909—January, 1954 R. & M. No. 2570 15*s.* (15*s.* 8*d.*)

Indexes to the Technical Reports of the Aeronautical Research Council—

December 1, 1936—June 30, 1939	R. & M. No. 1850	1*s.* 3*d.* (1*s.* 5*d.*)
July 1, 1939—June 30, 1945	R. & M. No. 1950	1*s.* (1*s.* 2*d.*)
July 1, 1945—June 30, 1946	R. & M. No. 2050	1*s.* (1*s.* 2*d.*)
July 1, 1946—December 31, 1946	R. & M. No. 2150	1*s.* 3*d.* (1*s.* 5*d.*)
January 1, 1947—June 30, 1947	R. & M. No. 2250	1*s.* 3*d.* (1*s.* 5*d.*)

Published Reports and Memoranda of the Aeronautical Research Council—

Between Nos. 2251–2349	R. & M. No. 2350	1*s.* 9*d.* (1*s.* 11*d.*)
Between Nos. 2351–2449	R. & M. No. 2450	2*s.* (2*s.* 2*d.*)
Between Nos. 2451–2549	R. & M. No. 2550	2*s.* 6*d.* (2*s.* 10*d.*)
Between Nos. 2551–2649	R. & M. No. 2650	2*s.* 6*d.* (2*s.* 10*d.*)
Between Nos. 2651–2749	R. & M. No. 2750	2*s.* 6*d.* (2*s.* 10*d.*)

Prices in brackets include postage

HER MAJESTY'S STATIONERY OFFICE

York House, Kingsway, London W.C.2; 423 Oxford Street, London W.1; 13a Castle Street, Edinburgh 2; 39 King Street, Manchester 2; 2 Edmund Street, Birmingham 3; 109 St. Mary Street, Cardiff; Tower Lane, Bristol 1; 80 Chichester Street, Belfast, *or through any bookseller.*

S.O. Code No. 23-3129